ARTICLE

Oocytes mount a noncanonical DNA damage response involving APC-Cdh1–mediated proteolysis

Goutham Narayanan Subramanian[1], Jessica Greaney[1], Zhe Wei[1], Olivier Becherel[2], Martin Lavin[2], and Hayden Anthony Homer[1]

In mitotic cells, DNA damage induces temporary G2 arrest via inhibitory Cdk1 phosphorylation. In contrast, fully grown G2-stage oocytes readily enter M phase immediately following chemical induction of DNA damage in vitro, indicating that the canonical immediate-response G2/M DNA damage response (DDR) may be deficient. Senataxin (Setx) is involved in RNA/DNA processing and maintaining genome integrity. Here we find that mouse oocytes deleted of Setx accumulate DNA damage when exposed to oxidative stress in vitro and during aging in vivo, after which, surprisingly, they undergo G2 arrest. Moreover, fully grown wild-type oocytes undergo G2 arrest after chemotherapy-induced in vitro damage if an overnight delay is imposed following damage induction. Unexpectedly, this slow-evolving DDR is not mediated by inhibitory Cdk1 phosphorylation but by APC-Cdh1–mediated proteolysis of the Cdk1 activator, cyclin B1, secondary to increased Cdc14B-dependent APC-Cdh1 activation and reduced Emi1-dependent inhibition. Thus, oocytes are unable to respond immediately to DNA damage, but instead mount a G2/M DDR that evolves slowly and involves a phosphorylation-independent proteolytic pathway.

Introduction

The overwhelming majority of oocytes in mammalian ovaries are arrested at G2 stage within primordial follicles (Greaney et al., 2018; Oktem and Urman, 2010). This is an unusually protracted arrest, lasting years in mice and decades in humans, during which time oocytes are vulnerable to DNA damage. How arrested oocytes avert DNA insults is the focus of intense investigation.

G2 arrest requires inhibition of cyclin-dependent kinase 1 (Cdk1) via inhibitory Thr14/Tyr15 phosphorylation mediated by Wee1/Myt1 kinases (Wee1B in oocytes) and counteracted by cell division cycle 25 (Cdc25) phosphatases (Adhikari et al., 2016; Adhikari and Liu, 2014; Han et al., 2005; Solc et al., 2010). In oocytes, Cdk1 inhibition also involves proteolysis of the Cdk1 activator, cyclin B1, orchestrated by the Cdh1-activated anaphase-promoting complex (APC-Cdh1; Holt et al., 2011; Homer, 2013; Reis et al., 2006).

The G2/M DNA damage response (DDR) in somatic cells delays cell cycle progression to enable DNA repair. This immediate response, which is short-lived and is relieved following DNA repair, involves a cascade of phosphorylation events brought about by the apical kinases, ATM (ataxia telangiectasia mutated) and ATR (ATM and RAD3-related), as well as downstream checkpoint kinases, checkpoint kinase 1 and 2 (Chk1/Chk2; Carroll and Marangos, 2013; Harper and Elledge, 2007). The latter induce

Cdc25 inhibition that prevents Cdk1 activation and M-phase entry. Cdk1 phospho-inhibition can be reinforced during mitosis by APC-Cdh1–mediated destruction of Polo-like kinase 1 (Plk1; Bassermann et al., 2008) although this response may occur only in certain cell lines or under certain experimental conditions (Wiebusch and Hagemeier, 2010). In the presence of longer-term genotoxic stress in some somatic cell types, APC-Cdh1–mediated targeting of a wider range of substrates including cyclin B1 occurs, leading to withdrawal from the cell cycle (Krenning et al., 2014; Müllers et al., 2014; Wiebusch and Hagemeier, 2010).

In mice, activated primordial follicles develop over weeks into primary, secondary, and ultimately, antral follicles, while at the same time, their contained oocytes undergo extensive growth (Greaney et al., 2018; Oktem and Urman, 2010). Following extreme chemotherapy/irradiation-induced injury in prepubertal female mice, primordial-stage oocytes activate TAp63 via ATM and Chk2 (Bolcun-Filas et al., 2014; Gonfloni et al., 2009; Livera et al., 2008; Suh et al., 2006; Tuppi et al., 2018). This triggers primordial follicle apoptosis via Puma and Noxa, resulting in premature depletion of the follicular pool and infertility (Kerr et al., 2012). Significantly, however, knockout or inhibition of TAp63, Chk2, Puma, or Noxa rescues primordial follicle survival following exogenously induced damage (Bolcun-Filas et al., 2014;

Kerr et al., 2012; Nguyen et al., 2018; Rinaldi et al., 2017; Suh et al., 2006), and knockout mice go on to have pups (Bolcun-Filas et al., 2014; Kerr et al., 2012), demonstrating that oocytes possess extensive DNA repair capacity.

Both primordial and fully grown oocytes from reproductively aged females exhibit higher levels of DNA breaks than young oocytes (Titus et al., 2013) indicating that physiological levels of primordial oocyte injury (as opposed to drug- or radiation-induced) do not necessarily trigger DDR-mediated apoptosis and can persist during folliculogenesis and oocyte growth, culminating in damaged fully grown oocytes. In keeping with bypass of TAp63-mediated apoptosis at milder degrees of injury, most primordial follicles survive the mild oocyte DNA damage induced by low doses of irradiation (0.1 Gy), which only partially activates TAp63 (Suh et al., 2006). In contrast, full activation of TAp63 at high irradiation doses (0.45 Gy) causes virtually all oocytes to succumb (Suh et al., 2006). DNA breaks are more likely to remain unrepaired in aged oocytes owing to reduced expression of DNA repair genes such as ATM, BRCA1, and RAD51 (Titus et al., 2013; Winship et al., 2018). Consistent with this, oocytes from mice with reduced BRCA1 expression or disrupted RAD51 function exhibit increased DNA damage (Kujjo et al., 2010; Titus et al., 2013; Winship et al., 2018). Thus, low levels of DNA damage may persist throughout oocyte growth without inducing apoptosis, especially when DNA repair capacity is compromised.

Damaged fully grown oocytes pose the greatest threat to pregnancy, since only fully grown oocytes are competent to undergo maturation and fertilization. Understanding how fully grown G2-stage oocytes respond to physiologically acquired DNA damage is therefore of paramount importance. Studies investigating the G2/M DDR in fully grown oocytes have predominantly used a model of in vitro treatment with chemotherapeutic drugs. In this model, fully grown and DNA-intact oocytes isolated from antral follicles are subjected to severe and short-lived treatment (1–3 h) with genotoxic agents (Collins and Jones, 2016; Collins et al., 2015; Marangos and Carroll, 2012; Marangos et al., 2015; Mayer et al., 2016). Despite incurring severe damage, these oocytes enter M phase with minimal disruption, showing that the G2/M DDR in grown oocytes is unable to mount an immediate response (Collins and Jones, 2016; Collins et al., 2015; Marangos and Carroll, 2012; Marangos et al., 2015; Mayer et al., 2016). Significantly, however, DNA damage arising in vivo persists much longer during oocyte growth, and it is not known whether longer-term damage might elicit a different response.

The SETX gene encodes a putative RNA:DNA helicase, Senataxin (Setx), which is mutated in the rare neurological disorders ataxia oculomotor apraxia type 2 (AOA2) and amyotrophic lateral sclerosis (Lavin et al., 2013). Like genes mutated in other neurodegenerative disorders, SETX protects the genome against DNA damage (Lavin et al., 2013). Notably, Setx-deficient fibroblast and lymphoblastoid cell lines derived from AOA2 patients are particularly vulnerable to oxidative stress–induced DNA damage, supporting an important role for Setx in repairing DNA double-strand breaks (DSBs) brought about by reactive oxygen species (ROS; Suraweera et al., 2007). Cells defective for SETX also exhibit defects in transcription

termination and the resolution of RNA:DNA hybrids (R-loops) arising at transcription pause sites (Lavin et al., 2013). In male mice lacking SETX, meiotic DSBs destined for recombination repair during prophase I of spermatogenesis persist due to unresolved R-loops leading to spermatocyte apoptosis and sterility (Becherel et al., 2013). Here we studied oocytes from female Setx-deficient mice for the first time. Consistent with Setx's role in protecting against ROS-induced DNA breaks (Suraweera et al., 2007), we find that in oocytes from Setx knockout female mice (Becherel et al., 2013), DNA breaks accumulate as oxidative stress increases both in vitro and during natural aging in vivo. Using this model of delayed acquisition of DNA damage, we here analyze the G2 DDR of fully grown oocytes.

Results

Loss of Setx does not affect oocyte maturation in young mice

We used a constitutive Setx knockout (Setx$^{-/-}$) mouse (Becherel et al., 2013; Fig. S1 a) and confirmed that mutant oocytes lack Setx expression (Fig. S1, b–d). We found that similar numbers of fully grown G2-arrested (germinal vesicle [GV]-stage) oocytes were isolated from hormonally primed 2–4-mo-old wild-type (Setx$^{+/+}$) and Setx$^{-/-}$ animals (Fig. 1 a). We measured the extent of DNA damage by immunostaining for γH2AX (phosphorylated histone H2 member X), a well-established marker of DSBs (Burma et al., 2001; Rogakou et al., 1998), and found comparable γH2AX levels in isolated fully grown Setx$^{-/-}$ and Setx$^{+/+}$ oocytes (Fig. 1, b and c).

Next, we analyzed meiotic maturation using time-lapse imaging and found that Setx$^{-/-}$ oocytes underwent GV breakdown (GVBD; marking entry into first meiotic M phase) and first polar body extrusion (marking exit from first meiotic M phase) at high rates (70–80%) similar to Setx$^{+/+}$ oocytes (Fig. 1, d and e). Moreover, time-lapse analyses of chromosome and spindle behavior using histone 2B (H2B)-RFP and silicon rhodamine (SiR)-tubulin (Wei et al., 2018), did not identify any differences in spindle assembly, chromosome alignment, or chromosome segregation between Setx$^{+/+}$ and Setx$^{-/-}$ oocytes (Fig. 1 f). Thus, in young animals, the numbers of fully grown oocytes and their maturation remain intact following loss of Setx.

These data also show that, unlike the need for Setx during meiotic recombination in males (Becherel et al., 2013), in females, recombination remains intact without Setx; otherwise, spindle structure, chromosome alignment, and meiotic progression would be grossly perturbed (Woods et al., 1999). Interestingly, therefore, these data reveal a sexually dimorphic requirement for SETX in gamete development, being essential in males (Becherel et al., 2013) but dispensable in young females.

Gradual emergence of DNA damage in vitro in Setx$^{-/-}$ oocytes induces G2 arrest

The foregoing showed that Setx$^{-/-}$ oocytes from young mice do not inherently possess increased levels of DNA damage. Because Setx is known to protect against oxidative stress–induced DNA damage (Suraweera et al., 2007), we next asked whether loss of Setx might predispose to increased damage when exposed to oxidative stress. We found that after overnight in vitro culture
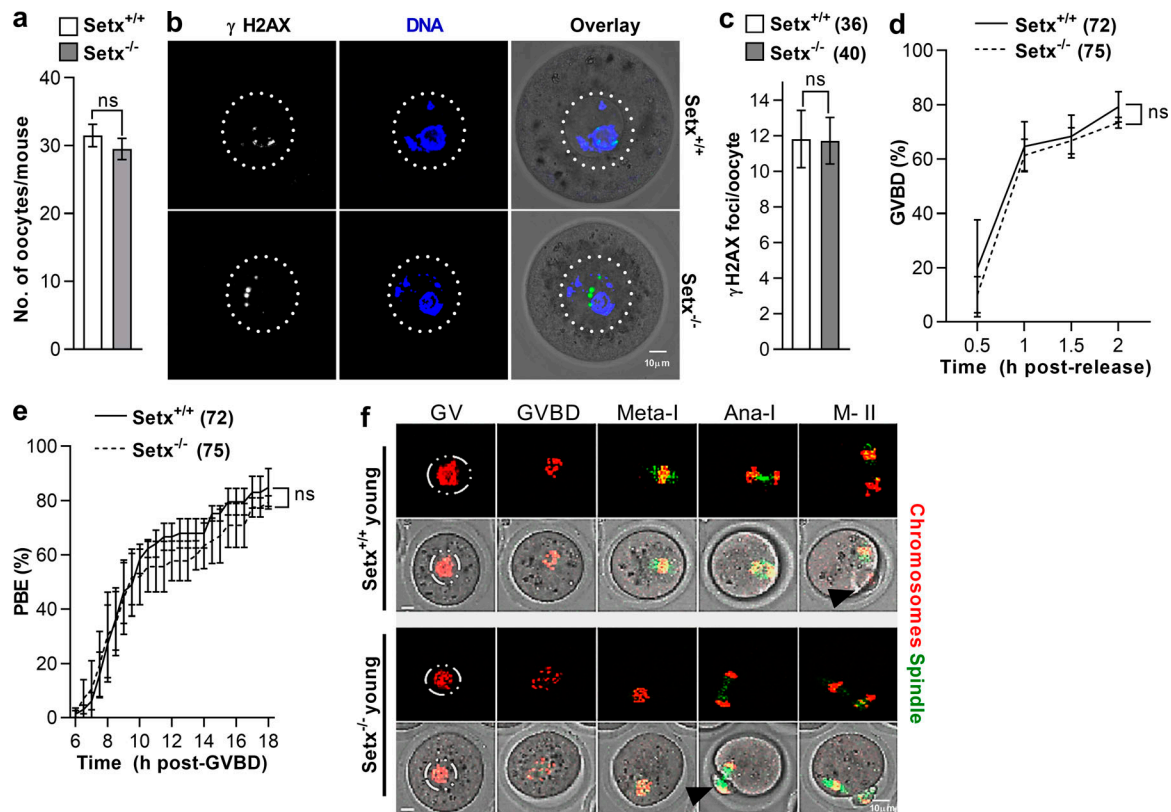
Subramanian et al.
Oocytes possess a G2/M DNA damage checkpoint

Journal of Cell Biology   2 of 14
https://doi.org/10.1083/jcb.201907213

Figure 1. **Loss of Setx does not affect oocyte maturation in young mice. (a)** Quantification of fully grown GV-stage oocytes per mouse (six mice per genotype). **(b and c)** Representative images of γH2AX and DNA labeling in fully grown Setx$^{+/+}$ and Setx$^{-/-}$ oocytes (b) and quantification of γH2AX-intensity per oocyte (c). **(d and e)** GVBD (d) and first polar body extrusion (PBE; e) rates of oocytes from Setx$^{+/+}$ and Setx$^{-/-}$ mice (four mice per genotype). **(f)** Representative time-lapse series of young Setx$^{+/+}$ and Setx$^{-/-}$ oocytes at GV, shortly after GVBD, followed by metaphase I, anaphase I, and metaphase II arrest (M-II). Black arrows depict the first polar body. Scale bars, 10 µm. Oocyte numbers are shown in parentheses from a minimum of three independent experiments. Error bars are mean ± SEM. Two-tailed Student's t test (a and c) or two-way ANOVA (d and e) was used for statistical analysis; ns, P > 0.05.

in 3-isobutyl-1-methylxanthine (IBMX), which maintains GV arrest, ROS levels increased markedly in both Setx$^{+/+}$ and Setx$^{-/-}$ oocytes (Fig. 2, a and b) consistent with known effects of in vitro culture (Halliwell, 2003; Martín-Romero et al., 2008). In keeping with Setx's role in protecting against oxidative damage, following overnight in vitro culture (hereafter referred to as ON oocytes), Setx$^{-/-}$-ON oocytes exhibited significantly higher levels of DNA damage than Setx$^{+/+}$-ON oocytes (Fig. 2, c and d). When oocytes were washed out of IBMX after overnight culture, GVBD rates were normal (~70–80% after 2 h) for Setx$^{+/+}$-ON oocytes with low levels of damage, but unexpectedly, were only ~40% for Setx$^{-/-}$-ON oocytes (Fig. 2 e).

Next, we investigated the cause for delayed M-phase entry in Setx$^{-/-}$-ON oocytes. To determine this, we cotreated Setx$^{+/+}$ and Setx$^{-/-}$ oocytes with either the antioxidant, N-acetyl cysteine (NAC), or DMSO during overnight culture in IBMX. Predictably, NAC-treated Setx$^{+/+}$ and Setx$^{-/-}$ oocytes exhibited lower ROS levels than DMSO-treated oocytes (Fig. 2, f and g). Importantly, NAC treatment also led to reduced DNA damage in Setx$^{-/-}$ oocytes (Fig. 2, h and i). Hence, increased DNA damage in Setx$^{-/-}$ oocytes is due to increased ROS, likely related to compromised repair of ROS-induced damage. Entirely in keeping with a repair function for Setx, DNA damage increased further with increasing time in culture (Fig. S2, a and b) in Setx$^{-/-}$ oocytes, whereas,

as we show later, chemically induced DNA damage in Setx$^{+/+}$ oocytes decreased as culture time increased (Fig. 3, f and g). Significantly, reducing DNA damage using NAC completely rescued GVBD in Setx$^{-/-}$-ON oocytes (Fig. 2 j). Thus, the G2/M delay in Setx$^{-/-}$-ON oocytes is not due to loss of Setx per se but to the increased DNA damage that develops because of reduced protection against oxidative stress.

Chemotherapy/irradiation-induced DNA damage induces G2 arrest after a delay

We were struck that DNA damage in Setx$^{-/-}$-ON oocytes significantly delayed M-phase entry since, based on the typical in vitro experimental model, it has been shown that fully grown oocytes do not immediately mount a DDR (Carroll and Marangos, 2013; Collins and Jones, 2016). Because G2 arrest can be triggered by extremely high levels of drug-induced damage (Marangos and Carroll, 2012), one explanation could be that Setx$^{-/-}$-ON oocytes acquired extremely high levels of DNA damage. To test this, we treated fully grown Setx$^{+/+}$ oocytes with etoposide (Eto) at the low end of the dose spectrum (10 µg/ml), which had previously been shown to have little impact on the G2-M transition (Marangos and Carroll, 2012). Consistent with earlier data, 10 µg/ml Eto had no discernible effects on GVBD if oocytes were released from IBMX immediately following drug
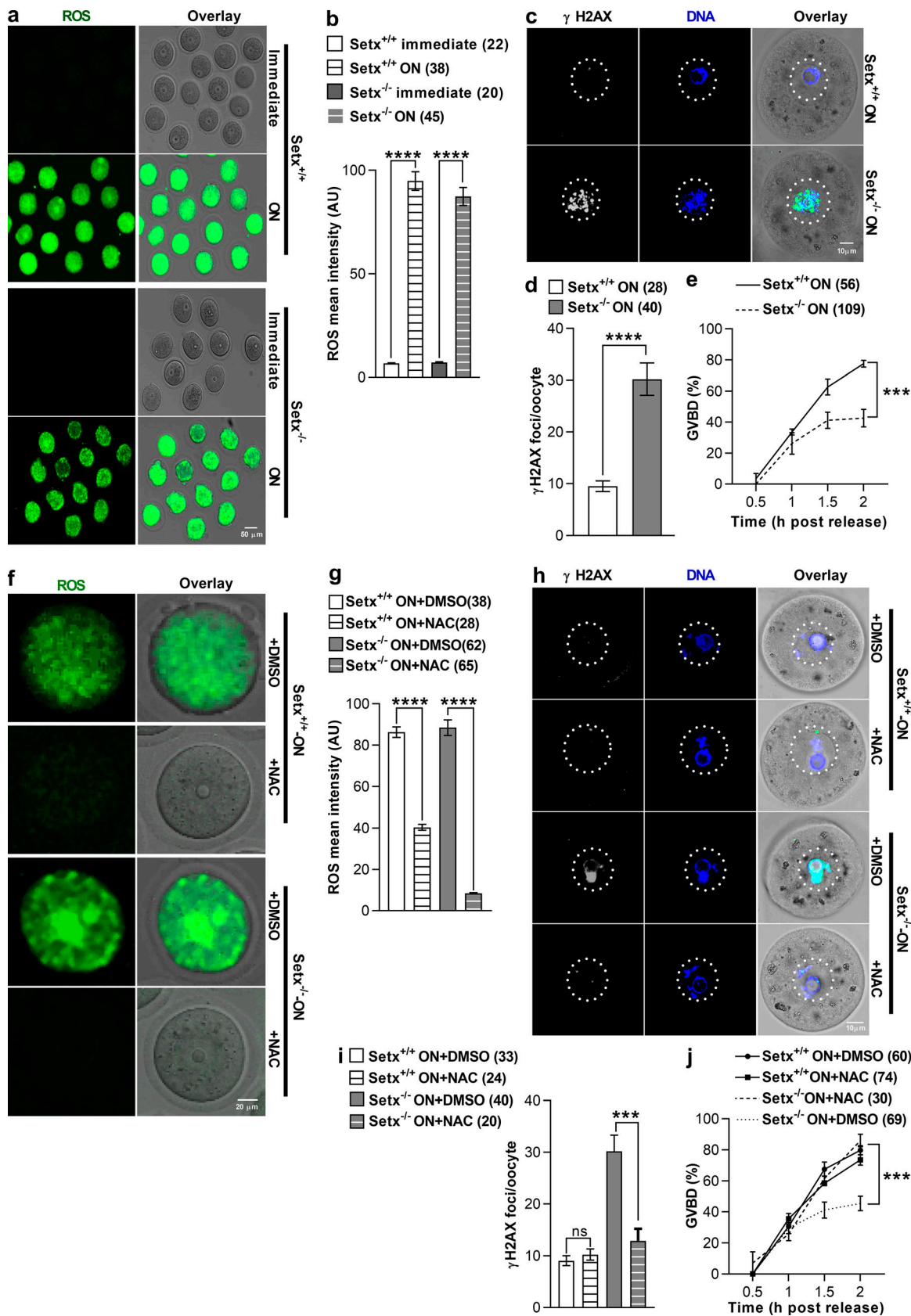
Figure 2. **Gradual emergence of DNA damage in Setx$^{-/-}$ oocytes induces G2 arrest. (a and b)** Representative images of ROS fluorescence in oocytes (a) and quantification of ROS levels in Setx$^{+/+}$ and Setx$^{-/-}$ oocytes immediately after harvesting (immediate) and after overnight culture (ON) in vitro (b). **(c and d)** Representative images of γH2AX and DNA labeling in Setx$^{+/+}$-ON and Setx$^{-/-}$-ON oocytes (c) and quantification of γH2AX-intensity per oocyte (d). **(e)** GVBD

Subramanian et al.
Oocytes possess a G2/M DNA damage checkpoint

Journal of Cell Biology   4 of 14
https://doi.org/10.1083/jcb.201907213

rates for Setx$^{+/+}$-ON and Setx$^{-/-}$-ON oocytes. **(f and g)** Representative images of ROS fluorescence (f) and quantification of ROS levels (g) in Setx$^{+/+}$-ON and Setx$^{-/-}$ oocytes treated with either DMSO or NAC during overnight culture (ON) in vitro. **(h and i)** Representative images of γH2AX and DNA labeling in Setx$^{+/+}$-ON and Setx$^{-/-}$-ON oocytes treated with either DMSO or NAC (h) and quantification of γH2AX-intensity per oocyte (i). **(j)** GVBD rates for Setx$^{+/+}$-ON and Setx$^{-/-}$-ON oocytes treated with either DMSO or NAC. Oocyte numbers are shown in parentheses from a minimum of three independent experiments. Error bars are mean ± SEM. Two-tailed Student's *t* test (b, d, g, and i) or two-way ANOVA (e and j) was used for statistical analysis. ***, P < 0.001; ****, P < 0.0001.

treatment (Fig. 3 d). Confusingly, however, we found that even at low Eto doses, DNA damage was markedly higher than in Setx$^{-/-}$-ON oocytes (Fig. 3, a and b), yet the latter underwent G2 arrest whereas the former did not. Thus G2 arrest in Setx$^{-/-}$-ON oocytes was not due to unusually high levels of DNA damage.

We noted that the time frame of damage induction in Setx$^{-/-}$-ON oocytes was markedly extended (>20 h) compared with the chemotherapy-based model (1–3 h), raising the possibility that a minimum amount of time may be required for the DDR to develop. If a DDR develops slowly in oocytes, we should also observe a G2/M defect using in vitro chemotherapy treatment if a delay is imposed after damage induction. We therefore compared M-phase entry in oocytes released from IBMX immediately following Eto treatment (hereafter termed Eto-immediate)

with those that were kept GV-arrested overnight (>20 h) in IBMX following Eto treatment (hereafter termed Eto-ON oocytes; Fig. 3 c). Although release from IBMX immediately after Eto treatment produced no delay in M-phase entry, consistent with previous reports (Marangos and Carroll, 2012), remarkably, GVBD rates for Eto-ON oocytes were reduced by ∼60% (Fig. 3 d). We obtained very similar results using another chemotherapeutic agent, doxorubicin (Fig. S2, c–e), as well as after induction of DSBs using UV irradiation (Fig. S2, f–h). Thus, three independent in vitro models demonstrate that oocytes mount a G2 arrest provided sufficient time is available for the DDR to develop.

Although GVBD rates for Eto-ON oocytes remained significantly reduced even 5 h following release from IBMX, increasing
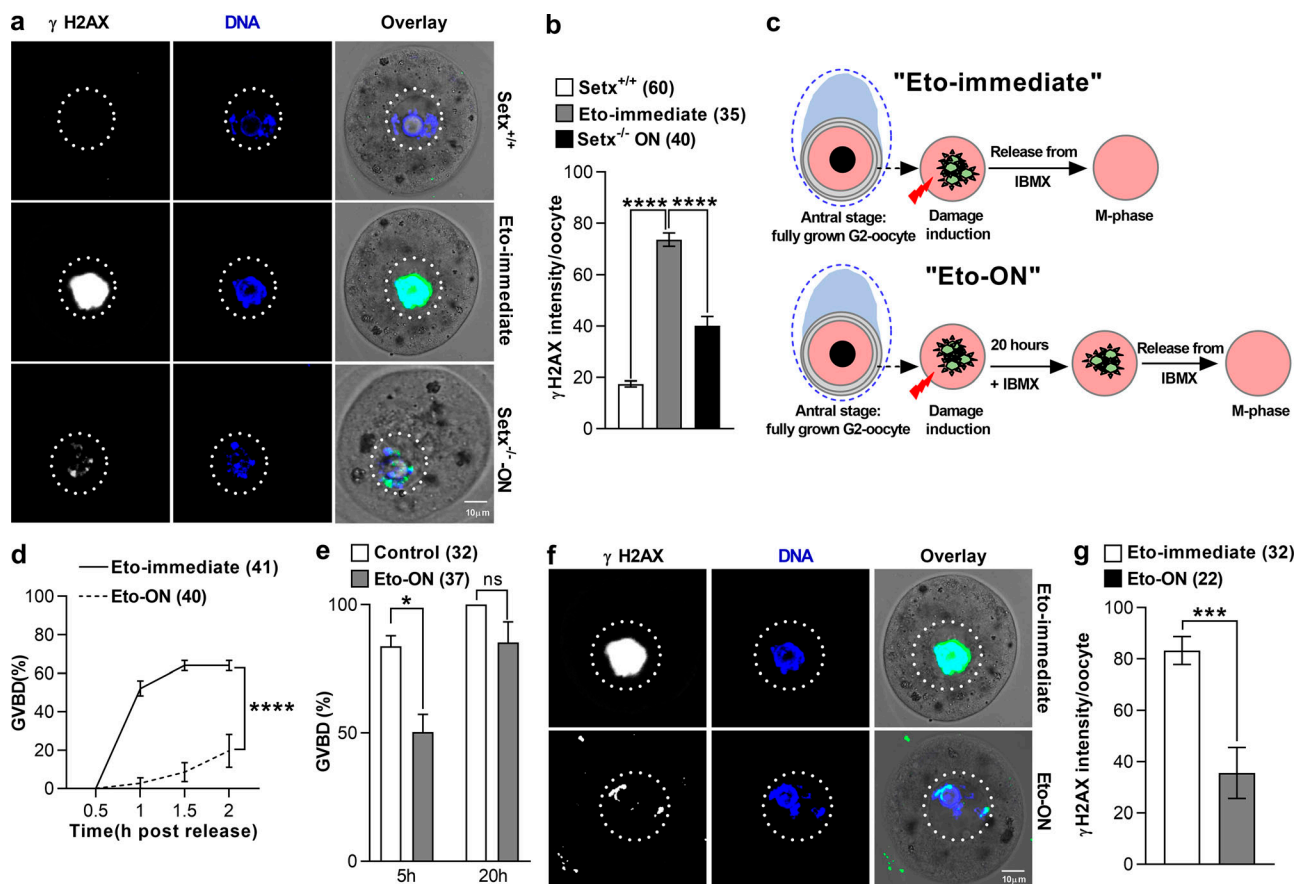

Figure 3. **Chemotherapy-induced DNA damage induces G2 arrest after a delay. (a and b)** Representative images of γH2AX and DNA labeling (a) and quantification of γH2AX intensity (b) in Setx$^{+/+}$ (untreated), Setx$^{+/+}$ oocytes immediately after treatment with Eto (Eto-immediate), and Setx$^{-/-}$-ON oocytes. **(c)** Schematic depicting experimental models of "Eto-immediate" and "Eto-ON" oocytes. **(d)** GVBD rates for Eto-immediate and Eto-ON oocytes. **(e)** GVBD rates 5 and 20 h after release from IBMX for DMSO-treated control and Eto-ON oocytes. **(f and g)** Representative images of γH2AX and DNA labeling (f) and quantification of γH2AX intensity (g) in Eto-immediate and Eto-ON oocytes. Oocyte numbers are shown in parentheses from a minimum of three independent experiments. Error bars are mean ± SEM. Two-tailed Student's *t* test (b, e, and g) or two-way ANOVA (d) was used for statistical analysis. ns, P > 0.05; *, P < 0.05; ***, P < 0.001; ****, P < 0.0001.

numbers of oocytes eventually underwent GVBD until, by 20 h, rates were similar to controls (Fig. 3 e). Notably, at the time of release from IBMX in Eto-ON oocytes, DNA repair was well underway (Fig. 3, f and g), explaining why GVBD rates eventually increased. Significantly therefore, the DDR we identify here invokes a transient meiotic delay responsive to DNA repair, distinguishing it from the permanent cell cycle withdrawal seen in some mitotic cells after prolonged genotoxic stress (Krenning et al., 2014; Wiebusch and Hagemeier, 2010).

DNA damage acquired in vivo during natural aging inhibits M-phase entry

Next, we sought to test whether the slow-response DDR that we identified using in vitro experiments might also occur in vivo. Given the crucial importance of Setx for combating ROS-induced damage and the well-known increase of cellular oxidative stress with aging (Lim and Luderer, 2011; Mihalas et al., 2017; Tarín, 1996; Titus et al., 2013), we investigated naturally aging mice. We found that by ~8 mo (which we refer to as "older"), fully grown Setx$^{+/+}$ and Setx$^{-/-}$ oocytes isolated from ovaries contained higher ROS levels than younger 2–4-mo-old mice (Fig. 4, a and b). Increased ROS was accompanied by more than fourfold higher levels of DNA damage in isolated fully grown Setx$^{-/-}$ compared with Setx$^{+/+}$ oocytes (Fig. 4, c and d). Notably, this damage seen in fully grown Setx$^{-/-}$ oocytes had likely been present during earlier stages of growth in vivo, since we found significantly more γH2AX-positive pre-antral and antral follicle-enclosed oocytes in older Setx$^{-/-}$ ovaries (Fig. 4, e and f). Significantly, in the presence of long-lived in vivo–acquired DNA damage in older Setx$^{-/-}$ oocytes, GVBD rates were approximately fourfold lower compared with older Setx$^{+/+}$ oocytes (Fig. 4 g). Thus, Setx$^{-/-}$ oocytes prematurely accumulate DNA damage in vivo during aging, in parallel with increasing oxidative stress. Furthermore, this long-lived DNA damage in vivo is associated with impaired M-phase entry.

The DDR in oocytes involves increased proteolysis

Short-term exposure to extremely high Eto doses (100 μg/ml) activates Cdk1 phosphoinhibitory pathways in mouse oocytes, whereas the lower doses we used here do not (Marangos and Carroll, 2012). We wondered whether the delayed-onset G2 arrest we observed in Setx$^{-/-}$-ON and Eto-ON oocytes was due to the canonical Cdk1 phosphoinhibitory pathway. We immunoblotted oocytes with an antibody specific for the inhibitory Cdk1 Tyr15 phospho-residue [p-Cdk1(Y15)]. Unexpectedly, we could not identify an increase in p-Cdk1(Y15) levels in either model (Fig. S3, a–d). We undertook further analyses in Eto-ON oocytes of key kinases in the canonical phosphorylation-mediated DDR upstream of p-Cdk1 and found no increase in either phosphorylated Chk1 or phosphorylated Chk2 (Fig. S3, e–g). Altogether, these data unexpectedly indicated that the delayed-response DDR associated with milder injury we identify here was not being mediated by canonical Cdk1 phosphoinhibition.

APC-Cdh1–mediated proteolysis occurs in response to DNA damage in mitotic cells (Bassermann et al., 2008; Wiebusch and Hagemeier, 2010). We were interested in the association between the DDR and proteolysis because, uniquely in GV-stage oocytes, APC-Cdh1 is constitutively active and degrades cyclin B1 to sustain G2 arrest (Holt et al., 2011; Homer, 2013; Homer et al., 2009; Marangos and Carroll, 2008; Reis et al., 2006). To investigate proteolysis in response to DNA damage, we undertook time-lapse imaging of fluorescently labeled cyclin B1 (cyclin B1-GFP) as before (Marangos and Carroll, 2008; Reis et al., 2006). In Setx$^{+/+}$-ON control oocytes, we found that ~30% of cyclin B1-GFP was degraded within 5 h (Fig. 5 a). Strikingly, in Setx$^{-/-}$-ON oocytes, more than twice as much cyclin B1-GFP was destroyed over the same 5-h period (Fig. 5 a). This was not simply because of the loss of Setx, since proteolysis in Setx$^{-/-}$ oocytes was indistinguishable from that in Setx$^{+/+}$ oocytes if analyses occurred immediately after oocytes were isolated from ovaries (Fig. 5 b), consistent with our other data showing clearly that delayed M-phase entry in Setx$^{-/-}$-ON oocytes was due to DNA damage (Fig. 2). Similarly, when we compared proteolysis in Eto-ON oocytes with that in Eto-immediate oocytes, we found that significantly more proteolysis occurred in the former compared with the latter within 5 h (Fig. 5 c). We investigated other APC-Cdh1 substrates and found that securin, Plk1, and Aurora kinase B also appeared to undergo destruction in Setx$^{-/-}$-ON and Eto-ON oocytes (Fig. S4). Thus, proteolysis increased if a delay occurred following DNA damage.

We reasoned that increased proteolysis could inhibit GVBD in oocytes by reducing the levels of Cdk1's activating subunit, cyclin B1 (Reis et al., 2006). This was indeed the case, since Western blotting showed that cyclin B1 levels were reduced in Setx$^{-/-}$-ON oocytes compared with Setx$^{+/+}$-ON oocytes and in Eto-ON oocytes compared with Eto-immediate oocytes (Fig. 5, d–g). To test whether reduced cyclin B1 secondary to destruction was important for delayed M-phase entry, we expressed a nondestructible cyclin B1-RFP construct (ND-cyclin B1-RFP; Gavet and Pines, 2010) in both Setx$^{-/-}$-ON and Eto-ON oocytes. Significantly, we found that in both cases, ND-cyclinB1-RFP markedly increased GVBD compared with RFP only (Fig. 5, h and i). Thus, increased proteolysis is important for inhibiting M-phase entry in damaged fully grown oocytes.

APC-Cdh1 mediates increased proteolysis with DNA damage

To determine whether APC-Cdh1 was responsible for increased proteolysis in response to DNA damage, we depleted Cdh1 using a validated CDH1-targeting morpholino, Cdh1MO (Homer et al., 2009; Reis et al., 2006; Fig. S5, a and b). We found that increased proteolysis previously seen in Setx$^{-/-}$-ON oocytes was almost completely abolished following depletion of Cdh1 (Fig. 6 a), leading to a complete rescue of GVBD (Fig. 6 b). Entirely consistent with this, we found that proteolysis was also blunted in Eto-ON oocytes following Cdh1 depletion (Fig. 6 c). This suggested that delayed M-phase entry in response to DNA damage was due to increased APC-Cdh1 activity. If this were so, then inhibiting the 26S proteasome, which acts downstream of APC-Cdh1, should produce a similar effect to Cdh1 depletion. In line with this prediction, we found that proteolysis was also severely inhibited in Eto-ON oocytes treated with the 26S proteasome inhibitor, MG132, but not with DMSO treatment (Fig. 6 d). Thus, increased proteolysis in Setx$^{-/-}$-ON and Eto-ON oocytes is mediated by APC-Cdh1.
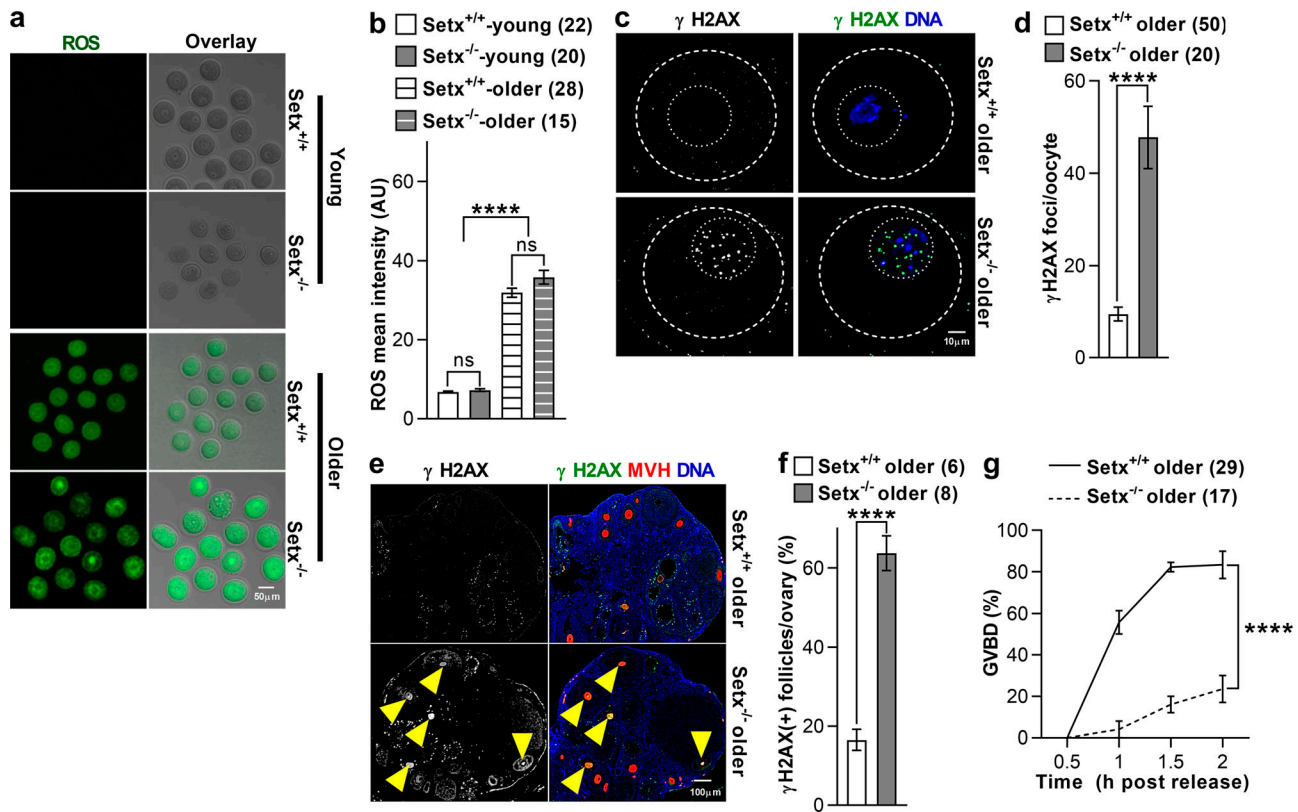
Subramanian et al.
Oocytes possess a G2/M DNA damage checkpoint

Journal of Cell Biology   6 of 14
https://doi.org/10.1083/jcb.201907213

Figure 4. DNA damage acquired in vivo during natural aging inhibits M-phase entry. (a and b) Representative images of ROS fluorescence in oocytes (a) and quantification of ROS levels (b) in young and older Setx⁺/⁺ and Setx⁻/⁻ oocytes immediately after harvesting. **(c and d)** Representative images of γH2AX and DNA labeling (c) and quantification of γH2AX-intensity (d) in Setx⁻/⁻-older oocytes. **(e and f)** Representative images of γH2AX, MVH, and DNA labeling (e) and quantification of proportion of γH2AX-positive follicles (f). MVH is a germ cell–specific marker (Toyooka et al., 2000) that was used for identifying oocytes. **(g)** GVBD rates for Setx⁺/⁺-older and Setx⁻/⁻-older oocytes. Oocyte numbers are shown in parentheses from a minimum of three independent experiments. Error bars are mean ± SEM. Two-tailed Student's *t* test (b, d, and f) or two-way ANOVA (g) was used for statistical analysis. ns, P > 0.05; ****, P < 0.0001.

We then asked how the delayed increase in APC-Cdh1 activity might come about. We immunoblotted Cdh1 levels in Eto-immediate and Eto-ON oocytes but did not find that Cdh1 levels changed (Fig. S5, c and d). In U2OS mitotic cells, APC-Cdh1 activation in response to DNA damage is secondary to increased Cdc14B phosphatase activity (Bassermann et al., 2008). In oocytes, Cdc14B also has an APC-Cdh1–activating function (Schindler and Schultz, 2009). To test whether Cdc14B activity might be responsible for increased APC-Cdh1 activity, we knocked down Cdc14B using siRNAs (Fig. S5, e and f). Significantly, proteolysis in Eto-ON oocytes was severely blunted by Cdc14B knockdown, but not by control siRNAs, and was associated with a significant increase in GVBD (Fig. S5, g and h).

Emi1 negatively regulates APC-Cdh1 at the G2-M boundary in oocytes (Marangos et al., 2007), and following longer-term genotoxic stress in somatic cells, Emi1 levels are reduced coincident with APC-Cdh1 activation (Wiebusch and Hagemeier, 2010). We therefore asked whether Emi1 might be involved in regulating APC-Cdh1 following DNA damage in oocytes. Strikingly, we found that Emi1 levels were markedly reduced in Setx⁻/⁻-ON and Eto-ON oocytes (Fig. 7, a–d). If reduced Emi1 levels contributed to increased APC-Cdh1 activity, then expression of exogenous Emi1-Venus (Di Fiore and Pines, 2007) should counter this to stabilize cyclin B1 and increase GVBD. Consistent

with an APC-Cdh1 inhibitory effect, we found that Emi1-Venus overexpression induced escape from IBMX-mediated arrest in ~20% of wild-type oocytes (Fig. 7 e). Significantly, in Eto-ON oocytes, Emi1-Venus rescued GVBD rates and increased cyclin B1 levels (Fig. 7, e–g).

Taken together, these data support that Cdc14B's activity increases while Emi1's decreases following DNA damage, thereby increasing APC-Cdh1–mediated cyclin B1 proteolysis to delay GVBD. Notably, substantial rescue of GVBD by ND-cyclin B1-RFP (Fig. 5, h and i) further supports that a separate pathway from inhibitory Cdk1 phosphorylation is responsible for preventing M-phase entry.

Discussion

Here we find that oocytes mount a DDR at the G2/M boundary that transiently delays M-phase entry. Crucially, this DDR evolves over several hours following the initial insult and differs from the canonical immediate-response DDR. Our findings are supported by an in vivo model and three separate in vitro models. We propose that within ovaries in vivo, where Cdk1 is constitutively suppressed within the inhibitory follicular environment (Adhikari and Liu, 2014; Solc et al., 2010), DNA repair capacity, rather than an immediate-response DDR, is critical for
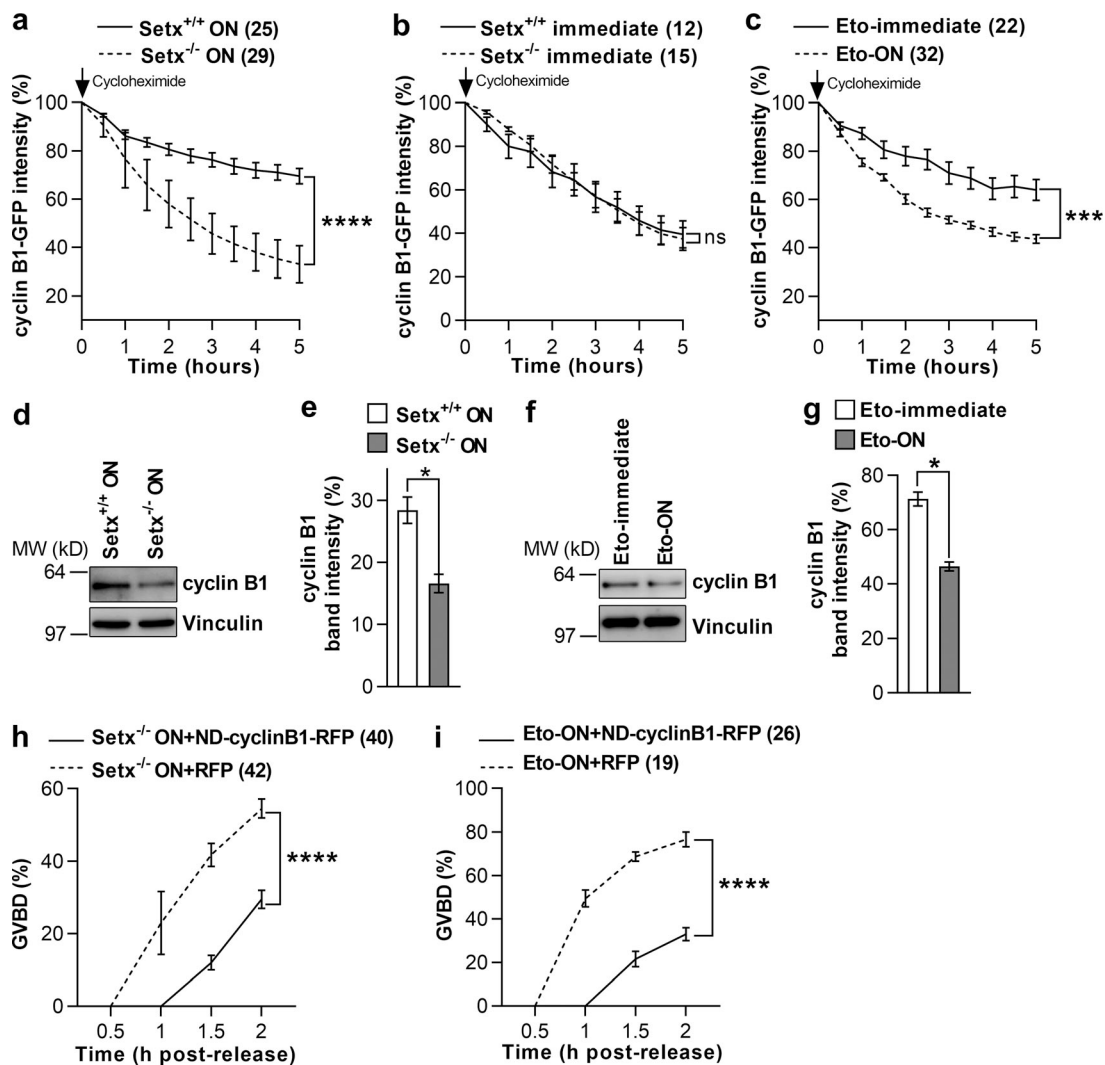
Subramanian et al.
Oocytes possess a G2/M DNA damage checkpoint

Journal of Cell Biology   7 of 14
https://doi.org/10.1083/jcb.201907213

Figure 5. **The DDR in oocytes involves increased proteolysis. (a–c)** Quantification of cyclin B1-GFP fluorescence decline in Setx^{+/+}-ON and Setx^{−/−}-ON (a), Setx^{+/+}-immediate and Setx^{−/−}-immediate (b), and Eto-immediate and Eto-ON (c) GV-stage oocytes. **(d and e)** Representative immunoblot (d) and quantification of cyclin B1 band intensities (e) in Setx^{+/+}-ON and Setx^{−/−}-ON oocytes (30 oocytes per lane). **(f and g)** Representative immunoblot (f) and quantification of cyclin B1 band intensities (g) in Eto-immediate and Eto-ON oocytes (30 oocytes per lane). **(h and i)** GVBD rates for Setx^{+/+}-ON (h) and Eto-ON (i) oocytes microinjected with either *RFP* or *ND-Cyclin B1-RFP* cRNA. Oocyte numbers are shown in parentheses from a minimum of three independent experiments. Error bars are mean ± SEM. Two-tailed Student's t test (e and g) or two-way ANOVA (a, b, c, h, and i) was used for statistical analysis. *, $P < 0.05$; ***, $P < 0.001$; ****, $P < 0.0001$; ns, $P > 0.05$. In immunoblots, vinculin served as a loading control.

averting insults. If, however, oocytes complete growth without finalizing DNA repair, their DDR is by that time capable of stalling entry into M phase. Indeed, this is exactly what we observe when DNA damage occurs in growing Setx^{−/−} oocytes in vivo as a result of aging-associated increases in oxidative stress (Fig. 4).

The G2/M DDR in somatic cells that induces a transient cell cycle arrest occurs shortly after damage induction and is mediated by Cdk1 phosphoinhibition (Fig. 8 a). In some somatic cell types, Cdk1 phosphoinhibition may incorporate APC-Cdh1–mediated Plk1 destruction (Bassermann et al., 2008), although this is by no means a universal phenomenon and depends on cell type (Wiebusch and Hagemeier, 2010). In contrast, the DDR we identify here in oocytes occurs after a delay and does not involve the canonical phosphorylation-dependent

pathway, relying instead on APC-Cdh1–mediated proteolysis of cyclin B1 (Fig. 8 b). Although APC-Cdh1–mediated proteolysis of cyclin B1 has been reported in some somatic cells after DNA damage, this response induces irreversible withdrawal from the cell cycle (Krenning et al., 2014; Müllers et al., 2014; Wiebusch and Hagemeier, 2010) distinct from the DDR that transiently delays mitosis (Fig. 8 a). Oocyte dependence on a proteolytic pathway is entirely consistent with a largely inactive ATM-dependent pathway in fully grown oocytes that can be artificially induced only by unusually severe damage (Marangos and Carroll, 2012) that, had it occurred in vivo, would have eliminated oocytes at the primordial stage via their ATM-Chk2-TAp63 pathway (Bolcun-Filas et al., 2014; Gonfloni et al., 2009; Livera et al., 2008; Suh et al., 2006; Tuppi et al., 2018).
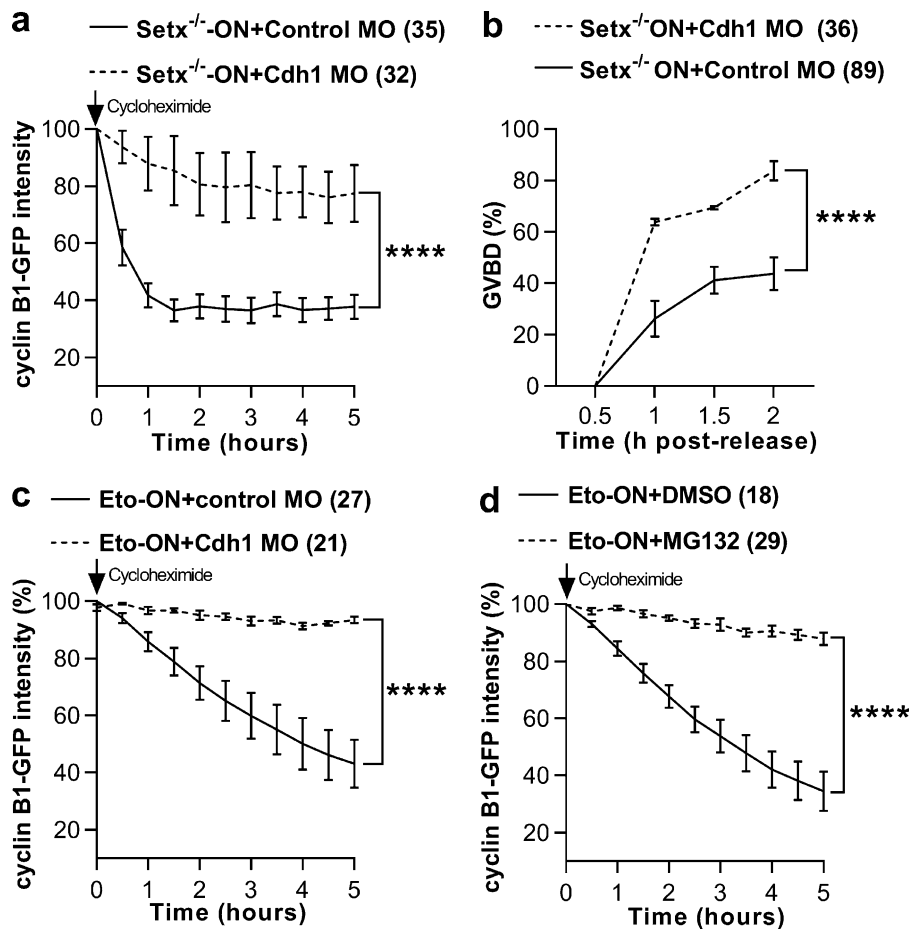
Figure 6. **APC-Cdh1 mediates increased proteolysis with DNA damage. (a)** Quantification of cyclin B1-GFP fluorescence decline in Setx$^{-/-}$-ON GV-stage oocytes that were either Cdh1 depleted or mock depleted. **(b)** GVBD rates for Setx$^{-/-}$-ON oocytes that were either Cdh1 depleted or mock depleted. **(c and d)** Quantification of cyclin B1-GFP fluorescence decline in Eto-ON GV-stage oocytes that were either Cdh1 depleted or mock depleted (c) and Eto-ON oocytes that were either DMSO treated (Control) or MG132 treated (d). Oocyte numbers are shown in parentheses from a minimum of three independent experiments. Error bars are mean ± SEM. Two-way ANOVA used for statistical analysis. ****, P < 0.0001.

Our data identify at least two causes for increased APC-Cdh1 activity, increased Cdc14B activity and reduced Emi1-mediated inhibition, both of which are known to increase APC-Cdh1 activity and inhibit M-phase entry in mouse oocytes (Marangos et al., 2007; Schindler and Schultz, 2009). We note that following DNA damage in mitosis, U2OS cells rely on a Cdc14B-dependent mechanism to activate APC-Cdh1 (Bassermann et al., 2008) whereas in HCT116 cells, Emi1 suppression seems to be important (Wiebusch and Hagemeier, 2010), leading to the proposition that the two mechanisms could be functionally redundant in somatic cells (Wiebusch and Hagemeier, 2010). Because APC-Cdh1 uniquely exhibits constitutive low-level activity in G2-arrested oocytes (Holt et al., 2011; Reis et al., 2006), this system may require both Cdc14B- and Emi1-dependent mechanisms to substantially increase proteolytic activity above an ongoing basal tone.

Findings in Setx$^{-/-}$ females differ drastically from Setx$^{-/-}$ males, in which loss of Setx results in persistent DNA breaks during recombination that activates a pachytene checkpoint, leading to elimination of spermatocytes and complete male sterility (Becherel et al., 2013). Interestingly, there have been case reports of premature ovarian insufficiency in AOA2 patients with *SETX* mutations (Lynch et al., 2007). Our findings suggest that this may occur due to compromised DNA repair capacity following Setx disruption, resulting in precocious accumulation of oocyte DNA damage and premature depletion of the ovarian reserve.

Materials and methods

Animals and generation of *SETX* knockouts

All animals were housed in a specific pathogen–free environment in filter-top cages and fed a standard diet. Experimental procedures were approved by the University Animal Ethics Committee.

SETX knockout mice were generated by targeted deletion of exon 4 of the *SETX* gene using a Cre-LoxP system as described previously (Becherel et al., 2013). In short, a targeting vector containing a neomycin-resistance (NeoR) cassette (Fig. S1 a) was derived from a bacterial artificial chromosome (BAC) clone corresponding to mouse chromosome 2 covering the *SETX* genomic sequence and transfected into ES cells. Successfully transfected ES cells were selected by antibiotic treatment with 150 µg/ml of G418 (Sigma-Aldrich; Becherel et al., 2013). C57BL6/129Sv mouse blastocysts were microinjected with NeoR-positive ES cells to generate chimeras. The NeoR cassette was then excised by crossing chimeras with *Cre*-expressing mice to generate Setx$^{-/-}$ mice containing only LoxP sites (Fig. S1 a). Setx$^{+/-}$ heterozygotes were mated to produce all three genotypes (*SETX*$^{+/+}$, *SETX*$^{+/-}$, and *SETX*$^{-/-}$).
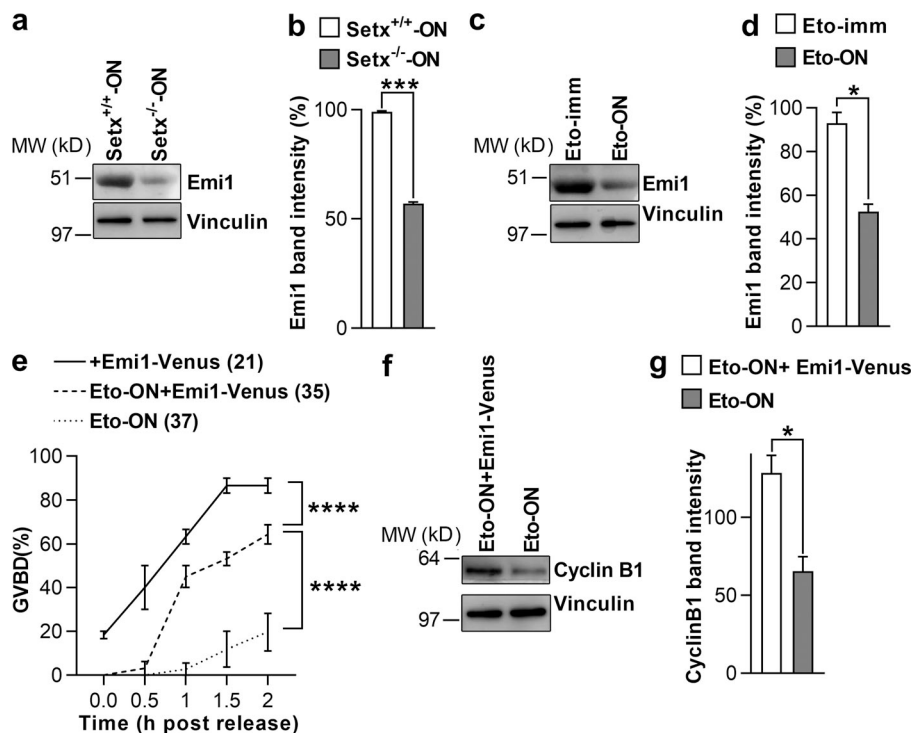
Figure 7. **Reduced Emi1 levels inhibit M-phase entry following DNA damage. (a and b)** Representative immunoblot (a) and quantification of Emi1 band intensities (b) in Setx$^{+/+}$-ON and Setx$^{-/-}$-ON oocytes (50 oocytes per lane). **(c and d)** Representative immunoblot (c) and quantification of Emi1 band intensities (d) in Eto-immediate and Eto-ON oocytes (50 oocytes per lane). **(e)** GVBD rates for oocytes microinjected with *EMI1-Venus* cRNA, Eto-ON oocytes microinjected with *EMI1-Venus* cRNA, and uninjected Eto-ON oocytes. Note that ∼20% of oocytes overexpressing Emi1-Venus overcame IBMX-mediated inhibition. **(f and g)** Representative immunoblot (f) and quantification of cyclin B1 band intensities (g) in Eto-ON oocytes with or without Emi1-venus overexpression (80 oocytes per lane). Oocyte numbers are shown in parentheses from a minimum of three independent experiments. Error bars are mean ± SEM. Two-tailed Student's *t* test (b, d, and g) or two-way ANOVA (e) was used for statistical analysis. *, P < 0.05; ***, P < 0.001; ****, P < 0.0001. In immunoblots, vinculin served as loading control.

Mice were weaned 21 d postpartum and ear notched for identification. Genotyping was performed using PCR on genomic DNA obtained from tail tips of 7–12-d-old mice. Tissue samples were lysed in a solution containing 150 µl of DirectPCR lysis reagent (Viagen) and 5 µl of 20 mg/ml Proteinase K (Thermo Fisher Scientific) at 55°C overnight on a rocking platform. The reaction was terminated by inactivating Proteinase K by heating samples at 85°C for 45 min. PCR reactions were set up with 1× GoTaq Green Master Mix (Promega), 1 µM of each of the three primers (ln3For, LoxpRev, and ln3Rev; Fig. S1 a), and nuclease-free water (Promega) to bring the reaction mixture to a final volume of 25 µl per sample. 1 µl of the DNA template was added to each sample before thermocycling. The sequences of primers used were ln3For: 5′-TTTAAGGAACAGTGCTGC-3′, ln3Rev: 5′-ATGAAGCAGGTAGGATTC-3′, and LoxPRev: 5′-CGA AGTTATATTAAGGGT-3′. PCR thermocycling conditions were as follows: denaturation at 95°C for 30 s, annealing at 49°C for 30 s and extension at 72°C for 1 min; 35 cycles; and a final extension at 72°C for 7 min. This protocol generated a 600-bp wild-type product and a 339-bp knockout product (Fig. S1, a and b). Samples from heterozygotes generated both products (a strong 600-bp band and a faint 339-bp band; Fig. S1 b).

Oocyte isolation, oocyte culture, and chemical treatment
Fully grown GV-stage oocytes were isolated from the ovaries of C57BL/6 female mice following hormonal priming with 7.5 IU of pregnant mare serum gonadotrophin (Intervet). Oocytes were handled in a Petri dish containing prewarmed M2 medium (Sigma-Aldrich) at 37°C supplemented with 100 µM of the phosphodiesterase inhibitor, IBMX (Sigma-Aldrich), which prevents oocytes from undergoing GVBD. Only fully grown cumulus-covered oocytes with clearly identifiable GVs were

used in experiments. Surrounding cumulus cells were mechanically denuded using mouth pipetting. To enable maturation, denuded GV-stage oocytes were washed through multiple droplets of M16 medium (Sigma-Aldrich) to remove all traces of IBMX. For longer-term culture, groups of oocytes were placed in dishes containing M16 microdroplets covered with mineral oil (Sigma-Aldrich) and incubated at 37°C in an atmosphere of 5% CO$_2$ in air.

DNA DSBs were induced by incubating oocytes in M16 medium containing either Eto (Sigma-Aldrich; 10 µg/ml) or doxorubicin (Hospira; 10 µg/ml) for 3 h or by exposure to UV-B radiation via a UV transilluminator (Vilber Lourmat; 312 nm) for 5 s. ROS production was attenuated by incubating oocytes overnight in M16 medium supplemented with NAC (5 mM; Abcam 139476). The 26S proteasome inhibitor, MG132 (SelleckChem; 5 µM), was used to inhibit proteolysis as described previously (Wei et al., 2018).

Microinjection, complementary RNA (cRNA) constructs, siRNAs, and morpholinos
Microinjection was performed as previously described (Gui and Homer, 2013; Homer et al., 2005a,b, 2009). Briefly, GV-stage oocytes in IBMX-treated medium were stabilized using suction applied through a hydraulic syringe to a prefabricated holding pipette (inner diameter 15 µm, outer diameter 75 µm, 35° bend; The Pipette Company). Microinjection needles were pulled from capillary tubes (0.86-mm inner diameter, 1.5-mm outer diameter; Harvard Apparatus) to a predetermined caliber using a vertical pipette puller (P30 vertical micropipette puller; Sutter Instruments). The tip of the microinjection pipette was advanced across the zona pellucida and oolemma into the cytoplasm of the oocyte, aided by a brief electrical pulse delivered by
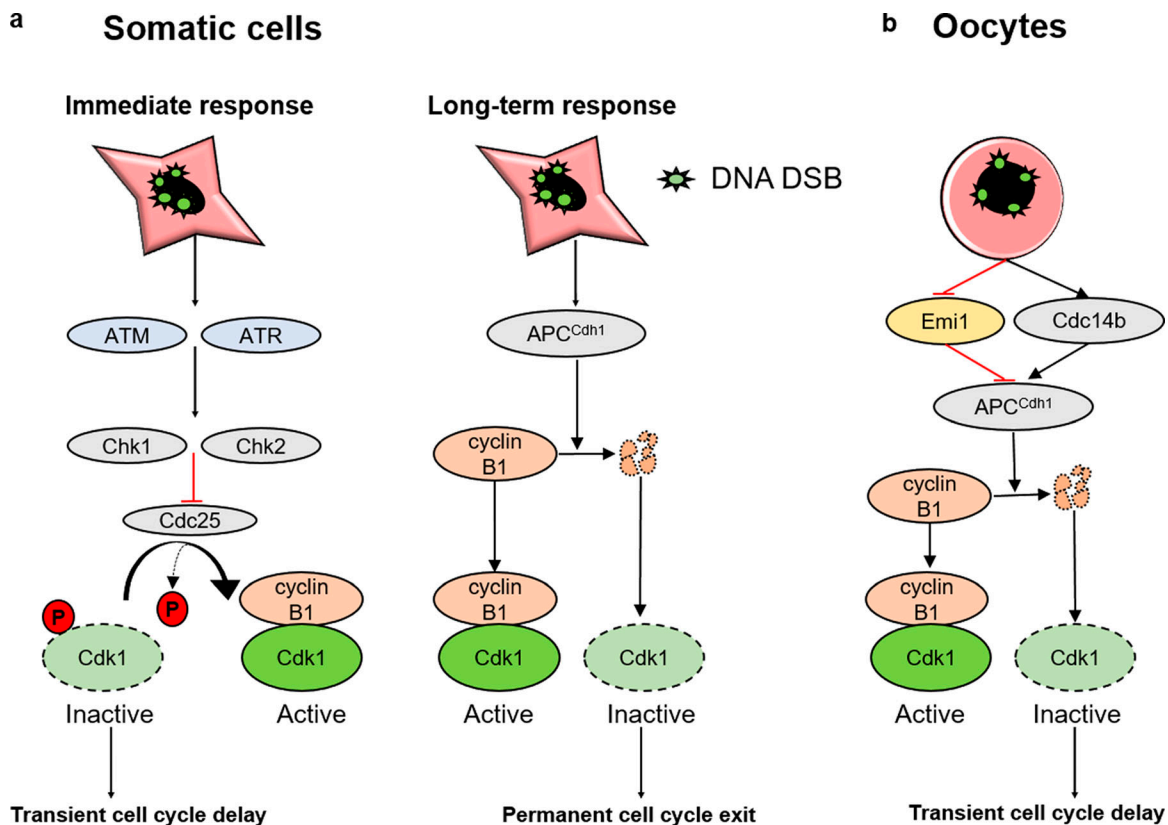
a Somatic cells

Immediate response   **Long-term response**

✸ DNA DSB

b Oocytes

Figure 8. **Schematic of G2/M DDR in somatic cells compared with oocytes. (a)** During mitosis, the downstream target of the immediate-response DDR that causes a transient delay in cell cycle progression to enable DNA repair is inhibitory Cdk1 phosphorylation. Mitotic cells mount another type of response to extended periods of genotoxic stress, which activates APC-Cdh1–mediated cyclin B1 destruction to cause irreversible withdrawal from the cell cycle. **(b)** In contrast, in oocytes, a transient DDR that furnishes time for DNA repair evolves slowly and does not target inhibitory Cdk1 phosphorylation but instead activates APC-Cdh1–mediated destruction of cyclin B1, thereby preventing Cdk1 activation required for entry into M phase.

an intracellular electrometer (IE-25IA; Warner Instruments). A precise volume roughly equal to 5% of the oocyte volume of test solution was then delivered to the oocyte using a Pneumatic PicoPump (PV-820; World Precision Instruments). The rate of oocyte death following microinjection was <10%.

The mMESSAGE mMACHINE High Yield Capped RNA Transcription kit (Ambion) was used to produce cRNA constructs by either T3 or T7 promoter–driven in vitro transcription from linearized DNA template as described previously; constructs used in this paper were H2B-RFP, Cyclin B1-GFP, and Emi1-mVenus (Di Fiore and Pines, 2007). All plasmids were fully sequenced before transcription. Following in vitro transcription, cRNA size was verified on agarose gels, and concentrations were determined using a spectrophotometer. Constructs were microinjected at the following concentrations: H2B-RFP at 250 ng/µl, Cyclin B1-GFP at 200 ng/µl, and Emi1-mVenus at 250 ng/µl. Following microinjection at the GV stage, oocytes were held in IBMX for ≥2 h to allow time for protein translation while maintaining GV arrest.

The siRNA sequences for targeting murine *CDC14B* were 5′-CAUUUAACCUUGACGAAUA-3′, 5′-GGCCAUGGUUUACAGAUA U-3′, 5′-GAAGACGCGUAUAGAACAU-3′, and 5′-GCAUAGAUA ACGAGCUAGA-3′ (siGENOME SMARTpool target sequences, Dharmacon). Control siRNA sequences were 5′-UUCUUCGAA

CGUGUCACGUTT-3′ and 5′-ACGUGACACGUUCGGAGAATT-3′ (Shanghai GenePharma). All siRNAs were injected at a final needle concentration of 50 µM.

Morpholino oligomer sequences (Gene Tools) for targeting murine *CDH1* (5′-CCTTCGCTCATAGTCCTGGTCCATG-3′) and a standard control morpholino (5′-CCTCTTACCTCATTACAATTT ATA-3′) have been described (Homer et al., 2009; Reis et al., 2006). Morpholinos were reconstituted to produce a final needle concentration of 17 µg/µl and a final oocyte concentration of 0.8 µg/µl. Morpholinos were activated by boiling at 90°C for 5 min before microinjection.

Immunoblotting

Western blotting was performed as described previously (Gui and Homer, 2012, 2013; Homer et al., 2009). Protein samples were prepared by washing oocytes with ultrapure water and lysing in LDS sample buffer (NuPAGE; Invitrogen). Samples were vigorously agitated and immediately snap-frozen at –80°C for storage until required. Samples were boiled at 95°C for 5 min following addition of reducing agent (NuPAGE). Proteins were separated on 4–12% Bis-Tris gels (NuPAGE; Invitrogen Australia) and transferred to PVDF membranes (Immobilon-P; Millipore). Following transfer, membranes were blocked for 1 h at room temperature in 3% BSA in TBS (25 mM Trizma base and 150 mM

sodium chloride) containing 0.05% Tween-20 (TBST). Primary antibody incubation was performed overnight at 4°C in blocking buffer. The primary antibodies used were p-Chk1 (Genetex, GTX100065; 1:1,000), p-Chk2 (R&D Systems, AF1626; 1:1,000), Cyclin B1 (Abcam, ab72; 1:400), Cdc14B (Abcam, ab203675; 1:500), Cdh1 (Abcam, ab3242; 1:200), p-Cdk1 (Cell Signaling, 9111S; 1:1,000), Emi1 (Thermo Fisher Scientific, 376600; 1:500), Plk1 (Abcam, ab17056; 1:500), Aurora Kinase B (Abcam, ab2254; 1:500), Securin (Abcam, ab3305; 1:200), and Vinculin (Sigma-Aldrich, V9131; 1:2,000). Following three 5-min washes in TBST, membranes were incubated in the appropriate HRP-conjugated goat anti-rabbit or goat anti-mouse secondary antibodies (1:1,000; Bio-Rad) for 1 h at room temperature. Chemiluminescence detection was performed using Western Lightning ECL-Pro (PerkinElmer) and imaged using Image Quant LAS500 (GE Healthcare).

Immunofluorescence
GV-stage oocytes were fixed as described previously (Gui and Homer, 2012, 2013; Homer et al., 2009). Briefly, oocytes were washed in Pipes, Hepes, EGTA, and MgCl₂ (PHEM) buffer (pH 7.0) and prepermeabilized in 0.25% Triton-X in PHEM. Oocytes were then fixed in 3.7% PFA solution in PHEM for 20 min. Oocytes were blocked overnight in 3% BSA in PBS containing 0.05% Tween-20 at 4°C. Primary antibody incubation with anti-γH2AX antibody (Abcam, ab11174; 1:200) and Cdc14B (Abcam, ab203675; 1:200) was performed for 1 h at 37°C. Primary antibody incubation with anti-Setx antibody (Suraweera et al., 2007; 1:200) was performed overnight at 4°C. Following three 5-min washes in PBS containing 0.5% BSA and 0.05% Tween-20, oocytes were incubated with the appropriate Alexa Fluor 488–conjugated secondary antibodies (1:200; Thermo Fisher Scientific) for 1 h at 37°C. Oocytes were then washed three times before staining for DNA by incubating in Hoechst 33342 (10 μg/ml; Sigma-Aldrich) for 5 min.

Immunohistochemistry
Ovaries were fixed in 4% PFA, embedded in paraffin (Thermo Shandon Histocentre 3), and sectioned serially at 3–4-μm thickness. The sections were placed on glass slides (Thermo Superfrost Plus) and incubated overnight at 37°C. The slides were rehydrated the following day using a Leica ST5010 Autostainer XL2, rinsed in distilled water for 2 min, and blocked in a solution containing 2% H₂O₂ for 10 min. Following two rinses in TBS, antigen retrieval was performed by incubating slides in Tris EDTA solution (pH 9.0) in a decloaking chamber for 5 min at 125°C. Sections were then blocked in 20% FCS, 2% BSA, and 0.2% Triton X-100 for 1 h at room temperature. Primary antibody incubation was performed in a humidified chamber for 30 min at room temperature in Da Vinci Green diluent (Biocare) containing either anti-γH2AX antibody (Abcam, ab11174; 1:1,500) or anti–mouse Vasa homologue (anti-MVH; Abcam, ab13840; 1:1,500). Following five 5-min washes in TBS containing 0.5% Triton X-100 at room temperature, slides were incubated in the appropriate secondary antibodies (PerkinElmer; 1:100) for 10 min at room temperature. Slides were then washed three times before staining DNA using Hoechst 33342 (10 μg/ml;

Sigma-Aldrich) for 10 min at room temperature. Following three 5-min washes, Menzel Glaser glass coverslips were applied (Thermo Fisher Scientific).

Images were captured using an upright fluorescence microscope (Axio Scope Imager M1; Carl Zeiss Microimaging) equipped with an EC Plan-Neofluar 10×/0.3-NA objective, a digital camera (Axio Cam 503 Mono; Carl Zeiss Microimaging), and appropriate dichroic filters. Quantification of follicles containing DNA breaks was performed by manually counting ovarian follicles in which there was clear colocalization of the MVH signal (for identifying oocytes) with γH2AX signals. Images captured in .czi file format were exported as .TIF files and assembled into panels using Adobe Illustrator (Adobe Systems).

ROS detection assay
ROS was detected using a commercial ROS Detection Assay Kit (Abcam, 139476; 10 μM). The assay was performed as per instructions provided with the kit. Briefly, GV-stage oocytes were incubated in the ROS detection reagent for 30 min in M16 medium supplemented with IBMX to prevent meiotic entry. The oocytes were washed through multiple droplets of M16 medium to remove any traces of the detection reagent and imaged immediately using confocal microscopy with the 488-nm laser line.

Confocal microscopy
Imaging was performed using a Leica TCS SP8 confocal microscope equipped with a 20×/0.75-NA Apochromat water-immersion objective fitted with an automated pump cap (water-immersion microdispenser, Leica; automated pump mp-x controller, Bartels Mikrotechnik) as described previously (Wei et al., 2018).

Images were imported from LAS X and analyzed using ImageJ software (National Institutes of Health). The region enclosing the GV was specified as a region of interest (ROI) and an automated Object Counter 3D plugin was used to count the number of γH2AX foci across a defined stack covering the entire GV region. γH2AX foci were considered signals exceeding a 25-voxel threshold using the threshold feature on the Object Counter 3D plugin.

Time-lapse microscopy was used to simultaneously image spindles and chromosomes (Wei et al., 2018). To visualize microtubules, SiR-Tubulin dye (Cytoskeleton) was added to medium at a final concentration of 100 nM as validated previously (Wei et al., 2018b). Oocytes were imaged in 1–2-μl microdrops of M16 medium in glass-bottom dishes (35 × 10-mm dish, no. 0 coverslip; MatTek) under mineral oil enclosed within a purpose-built stage-mounted incubation chamber designed to maintain conditions of 37°C and 5% CO₂ in air. Temperature fluctuation was further buffered by enclosing the entire microscope, including the stage-mounted chamber, in a custom-designed polycarbonate incubator (Life Imaging Services) that maintained a stable internal temperature of 37°C. Automated image capture was driven by Leica LAS X software. At the commencement of imaging, the positions of GVs in the z-axis were located. The complete stack was then derived by setting a stack thickness of 40 μm. Z-stacks were acquired with step intervals of 4 μm at 30-min intervals and a speed of 600 Hz. Using the Leica mark-and-find tool, we typically imaged multiple groups of oocytes in

separate droplets in each experiment. The 561-nm (for H2B-RFP) and 633-nm (for SiR-Tubulin) laser lines were used at 0.5% and 3% intensity, respectively.

Postacquisition image processing was performed using Leica LAS X, and images were assembled into panels using Adobe Illustrator. Fluorescence images were produced by Z-projecting the entire stack of fluorescence images from both channels and merging them with images in the bright-field channel.

For quantifying proteolysis, GV-stage oocytes were microinjected with cyclin B1-GFP cRNA and allowed to express protein for ≥2 h while being maintained in GV arrest using IBMX. GV-stage oocytes maintained in IBMX were then transferred to medium containing 10 µg/ml of cycloheximide to inhibit new protein synthesis from microinjected cyclin B1-GFP cRNA. In this way, any fluorescence intensity decline could be reliably attributed to proteolysis. Cyclin B1-GFP fluorescence was detected using the 488-nm laser line at 1% intensity. Z-stacks of 50-µm thickness were acquired with step intervals of 5 µm at 30-min intervals at a speed of 600 Hz. After importing LAS X images into ImageJ, a maximum-intensity projection of the entire Z-stack was performed, an ROI was drawn around the entire oocyte, and fluorescence intensity within this ROI was measured over time. Graphs of fluorescence intensity against time were then plotted to measure proteolysis.

Graphical representation and statistical analysis

Prism (GraphPad) was used to calculate mean and SEM. Statistical comparisons were made using either a two-tailed Student's *t* test with Welch's correction (for comparing two experimental groups) or two-way ANOVA (with Sidak's multiple comparisons test) as appropriate to the dataset. Data distribution was assumed to be normal, although this was not formally tested. Graphs were prepared in Prism. P values are represented as *, $P < 0.05$; **, $P < 0.01$; ***, $P < 0.001$; ****, $P < 0.0001$; and ns, $P > 0.05$. In figures, oocyte numbers are shown within parentheses. All experiments were repeated a minimum of three times.

Online supplemental material

Fig. S1 shows targeted deletion of the SETX gene and oocyte Setx expression. Fig. S2 shows DNA damage in Setx$^{-/-}$ oocytes during in vitro culture and response to treatment with either doxorubicin or UV-B irradiation. Fig. S3 shows that G2 arrest was not due to the canonical phosphorylation pathway. Fig. S4 shows reduced levels of APC-Cdh1 substrates in Setx$^{-/-}$-ON and Eto-ON oocytes. Fig. S5 shows morpholino-induced depletion of Cdh1, that Eto treatment does not affect Cdh1 levels, and that Cdc14B activity increases following DNA damage and inhibits M-phase entry.

Acknowledgments

Author contributions: H.A. Homer conceived the project and designed experiments. G.N. Subramanian conducted most experiments with assistance from J. Greaney, Z. Wei, and O. Becherel. M. Lavin generated the Setx knockout mice and provided intellectual support regarding Setx. G.N. Subramanian analyzed data, and G.N. Subramanian and H.A. Homer interpreted data. H.A. Homer wrote the manuscript. The final manuscript and data were made available to all authors for review and comment before submission.

References

Adhikari, D., and K. Liu. 2014. The regulation of maturation promoting factor during prophase I arrest and meiotic entry in mammalian oocytes. *Mol. Cell. Endocrinol.* 382:480–487. https://doi.org/10.1016/j.mce.2013.07.027

Adhikari, D., K. Busayavalasa, J. Zhang, M. Hu, S. Risal, M.B. Bayazit, M. Singh, M.K. Diril, P. Kaldis, and K. Liu. 2016. Inhibitory phosphorylation of Cdk1 mediates prolonged prophase I arrest in female germ cells and is essential for female reproductive lifespan. *Cell Res.* 26:1212–1225. https://doi.org/10.1038/cr.2016.119

Bassermann, F., D. Frescas, D. Guardavaccaro, L. Busino, A. Peschiaroli, and M. Pagano. 2008. The Cdc14B-Cdh1-Plk1 axis controls the G2 DNA-damage-response checkpoint. *Cell.* 134:256–267. https://doi.org/10.1016/j.cell.2008.05.043

Becherel, O.J., A.J. Yeo, A. Stellati, E.Y. Heng, J. Luff, A.M. Suraweera, R. Woods, J. Fleming, D. Carrie, K. McKinney, et al. 2013. Senataxin plays an essential role with DNA damage response proteins in meiotic recombination and gene silencing. *PLoS Genet.* 9:e1003435. https://doi.org/10.1371/journal.pgen.1003435

Bolcun-Filas, E., V.D. Rinaldi, M.E. White, and J.C. Schimenti. 2014. Reversal of female infertility by Chk2 ablation reveals the oocyte DNA damage checkpoint pathway. *Science.* 343:533–536. https://doi.org/10.1126/science.1247671

Burma, S., B.P. Chen, M. Murphy, A. Kurimasa, and D.J. Chen. 2001. ATM phosphorylates histone H2AX in response to DNA double-strand breaks. *J. Biol. Chem.* 276:42462–42467. https://doi.org/10.1074/jbc.C100466200

Carroll, J., and P. Marangos. 2013. The DNA damage response in mammalian oocytes. *Front. Genet.* 4:117. https://doi.org/10.3389/fgene.2013.00117

Collins, J.K., and K.T. Jones. 2016. DNA damage responses in mammalian oocytes. *Reproduction.* 152:R15–R22. https://doi.org/10.1530/REP-16-0069

Collins, J.K., S.I.R. Lane, J.A. Merriman, and K.T. Jones. 2015. DNA damage induces a meiotic arrest in mouse oocytes mediated by the spindle assembly checkpoint. *Nat. Commun.* 6:8553. https://doi.org/10.1038/ncomms9553

Di Fiore, B., and J. Pines. 2007. Emi1 is needed to couple DNA replication with mitosis but does not regulate activation of the mitotic APC/C. *J. Cell Biol.* 177:425–437. https://doi.org/10.1083/jcb.200611166

Gavet, O., and J. Pines. 2010. Progressive activation of CyclinB1-Cdk1 coordinates entry to mitosis. *Dev. Cell.* 18:533–543. https://doi.org/10.1016/j.devcel.2010.02.013

Gonfloni, S., L. Di Tella, S. Caldarola, S.M. Cannata, F.G. Klinger, C. Di Bartolomeo, M. Mattei, E. Candi, M. De Felici, G. Melino, and G. Cesareni. 2009. Inhibition of the c-Abl-TAp63 pathway protects mouse oocytes from chemotherapy-induced death. *Nat. Med.* 15:1179–1185. https://doi.org/10.1038/nm.2033

Greaney, J., Z. Wei, and H. Homer. 2018. Regulation of chromosome segregation in oocytes and the cellular basis for female meiotic errors. *Hum. Reprod. Update.* 24:135–161. https://doi.org/10.1093/humupd/dmx035

Gui, L., and H. Homer. 2012. Spindle assembly checkpoint signalling is uncoupled from chromosomal position in mouse oocytes. *Development.* 139:1941–1946. https://doi.org/10.1242/dev.078352

Gui, L., and H. Homer. 2013. Hec1-dependent cyclin B2 stabilization regulates the G2-M transition and early prometaphase in mouse oocytes. *Dev. Cell.* 25:43–54. https://doi.org/10.1016/j.devcel.2013.02.008

Halliwell, B. 2003. Oxidative stress in cell culture: an under-appreciated problem? *FEBS Lett.* 540:3–6. https://doi.org/10.1016/S0014-5793(03)00235-7

Subramanian et al.
Oocytes possess a G2/M DNA damage checkpoint

Journal of Cell Biology   13 of 14
https://doi.org/10.1083/jcb.201907213

Han, S.J., R. Chen, M.P. Paronetto, and M. Conti. 2005. Wee1B is an oocyte-specific kinase involved in the control of meiotic arrest in the mouse. *Curr. Biol.* 15:1670–1676. https://doi.org/10.1016/j.cub.2005.07.056

Harper, J.W., and S.J. Elledge. 2007. The DNA damage response: ten years after. *Mol. Cell.* 28:739–745. https://doi.org/10.1016/j.molcel.2007.11.015

Holt, J.E., S.M. Tran, J.L. Stewart, K. Minahan, I. García-Higuera, S. Moreno, and K.T. Jones. 2011. The APC/C activator FZR1 coordinates the timing of meiotic resumption during prophase I arrest in mammalian oocytes. *Development.* 138:905–913. https://doi.org/10.1242/dev.059022

Homer, H. 2013. The APC/C in female mammalian meiosis I. *Reproduction.* 146:R61–R71. https://doi.org/10.1530/REP-13-0163

Homer, H., L. Gui, and J. Carroll. 2009. A spindle assembly checkpoint protein functions in prophase I arrest and prometaphase progression. *Science.* 326:991–994. https://doi.org/10.1126/science.1175326

Homer, H.A., A. McDougall, M. Levasseur, K. Yallop, A.P. Murdoch, and M. Herbert. 2005a. Mad2 prevents aneuploidy and premature proteolysis of cyclin B and securin during meiosis I in mouse oocytes. *Genes Dev.* 19:202–207. https://doi.org/10.1101/gad.328105

Homer, H.A., A. McDougall, M. Levasseur, A.P. Murdoch, and M. Herbert. 2005b. Mad2 is required for inhibiting securin and cyclin B degradation following spindle depolymerisation in meiosis I mouse oocytes. *Reproduction.* 130:829–843. https://doi.org/10.1530/rep.1.00856

Kerr, J.B., K.J. Hutt, E.M. Michalak, M. Cook, C.J. Vandenberg, S.H. Liew, P. Bouillet, A. Mills, C.L. Scott, J.K. Findlay, and A. Strasser. 2012. DNA damage-induced primordial follicle oocyte apoptosis and loss of fertility require TAp63-mediated induction of Puma and Noxa. *Mol. Cell.* 48:343–352. https://doi.org/10.1016/j.molcel.2012.08.017

Krenning, L., F.M. Feringa, I.A. Shaltiel, J. van den Berg, and R.H. Medema. 2014. Transient activation of p53 in G2 phase is sufficient to induce senescence. *Mol. Cell.* 55:59–72. https://doi.org/10.1016/j.molcel.2014.05.007

Kujjo, L.L., T. Laine, R.J. Pereira, W. Kagawa, H. Kurumizaka, S. Yokoyama, and G.I. Perez. 2010. Enhancing survival of mouse oocytes following chemotherapy or aging by targeting Bax and Rad51. *PLoS One.* 5:e9204. https://doi.org/10.1371/journal.pone.0009204

Lavin, M.F., A.J. Yeo, and O.J. Becherel. 2013. Senataxin protects the genome: Implications for neurodegeneration and other abnormalities. *Rare Dis.* 1:e25230. https://doi.org/10.4161/rdis.25230

Lim, J., and U. Luderer. 2011. Oxidative damage increases and antioxidant gene expression decreases with aging in the mouse ovary. *Biol. Reprod.* 84:775–782. https://doi.org/10.1095/biolreprod.110.088583

Livera, G., B. Petre-Lazar, M.J. Guerquin, E. Trautmann, H. Coffigny, and R. Habert. 2008. p63 null mutation protects mouse oocytes from radio-induced apoptosis. *Reproduction.* 135:3–12. https://doi.org/10.1530/REP-07-0054

Lynch, D.R., C.D. Braastad, and N. Nagan. 2007. Ovarian failure in ataxia with oculomotor apraxia type 2. *Am. J. Med. Genet. A.* 143A:1775–1777. https://doi.org/10.1002/ajmg.a.31816

Marangos, P., and J. Carroll. 2008. Securin regulates entry into M-phase by modulating the stability of cyclin B. *Nat. Cell Biol.* 10:445–451. https://doi.org/10.1038/ncb1707

Marangos, P., and J. Carroll. 2012. Oocytes progress beyond prophase in the presence of DNA damage. *Curr. Biol.* 22:989–994. https://doi.org/10.1016/j.cub.2012.03.063

Marangos, P., E.W. Verschuren, R. Chen, P.K. Jackson, and J. Carroll. 2007. Prophase I arrest and progression to metaphase I in mouse oocytes are controlled by Emi1-dependent regulation of APC(Cdh1). *J. Cell Biol.* 176:65–75. https://doi.org/10.1083/jcb.200607070

Marangos, P., M. Stevense, K. Niaka, M. Lagoudaki, I. Nabti, R. Jessberger, and J. Carroll. 2015. DNA damage-induced metaphase I arrest is mediated by the spindle assembly checkpoint and maternal age. *Nat. Commun.* 6:8706. https://doi.org/10.1038/ncomms9706

Martín-Romero, F.J., E.M. Miguel-Lasobras, J.A. Domínguez-Arroyo, E. González-Carrera, and I.S. Alvarez. 2008. Contribution of culture media to oxidative stress and its effect on human oocytes. *Reprod. Biomed. Online.* 17:652–661. https://doi.org/10.1016/S1472-6483(10)60312-4

Mayer, A., V. Baran, Y. Sakakibara, A. Brzakova, I. Ferencova, J. Motlik, T.S. Kitajima, R.M. Schultz, and P. Solc. 2016. DNA damage response during mouse oocyte maturation. *Cell Cycle.* 15:546–558. https://doi.org/10.1080/15384101.2015.1128592

Mihalas, B.P., K.A. Redgrove, E.A. McLaughlin, and B. Nixon. 2017. Molecular Mechanisms Responsible for Increased Vulnerability of the Ageing Oocyte to Oxidative Damage. *Oxid. Med. Cell. Longev.* 2017:4015874. https://doi.org/10.1155/2017/4015874

Müllers, E., H. Silva Cascales, H. Jaiswal, A.T. Saurin, and A. Lindqvist. 2014. Nuclear translocation of Cyclin B1 marks the restriction point for terminal cell cycle exit in G2 phase. *Cell Cycle.* 13:2733–2743. https://doi.org/10.4161/15384101.2015.945831

Nguyen, Q.N., N. Zerafa, S.H. Liew, F.H. Morgan, A. Strasser, C.L. Scott, J.K. Findlay, M. Hickey, and K.J. Hutt. 2018. Loss of PUMA protects the ovarian reserve during DNA-damaging chemotherapy and preserves fertility. *Cell Death Dis.* 9:618. https://doi.org/10.1038/s41419-018-0633-7

Oktem, O., and B. Urman. 2010. Understanding follicle growth in vivo. *Hum. Reprod.* 25:2944–2954. https://doi.org/10.1093/humrep/deq275

Reis, A., H.Y. Chang, M. Levasseur, and K.T. Jones. 2006. APCcdh1 activity in mouse oocytes prevents entry into the first meiotic division. *Nat. Cell Biol.* 8:539–540. https://doi.org/10.1038/ncb1406

Rinaldi, V.D., K. Hsieh, R. Munroe, E. Bolcun-Filas, and J.C. Schimenti. 2017. Pharmacological Inhibition of the DNA Damage Checkpoint Prevents Radiation-Induced Oocyte Death. *Genetics.* 206:1823–1828. https://doi.org/10.1534/genetics.117.203455

Rogakou, E.P., D.R. Pilch, A.H. Orr, V.S. Ivanova, and W.M. Bonner. 1998. DNA double-stranded breaks induce histone H2AX phosphorylation on serine 139. *J. Biol. Chem.* 273:5858–5868. https://doi.org/10.1074/jbc.273.10.5858

Schindler, K., and R.M. Schultz. 2009. CDC14B acts through FZR1 (CDH1) to prevent meiotic maturation of mouse oocytes. *Biol. Reprod.* 80:795–803. https://doi.org/10.1095/biolreprod.108.074906

Solc, P., R.M. Schultz, and J. Motlik. 2010. Prophase I arrest and progression to metaphase I in mouse oocytes: comparison of resumption of meiosis and recovery from G2-arrest in somatic cells. *Mol. Hum. Reprod.* 16:654–664. https://doi.org/10.1093/molehr/gaq034

Suh, E.K., A. Yang, A. Kettenbach, C. Bamberger, A.H. Michaelis, Z. Zhu, J.A. Elvin, R.T. Bronson, C.P. Crum, and F. McKeon. 2006. p63 protects the female germ line during meiotic arrest. *Nature.* 444:624–628. https://doi.org/10.1038/nature05337

Suraweera, A., O.J. Becherel, P. Chen, N. Rundle, R. Woods, J. Nakamura, M. Gatei, C. Criscuolo, A. Filla, L. Chessa, et al. 2007. Senataxin, defective in ataxia oculomotor apraxia type 2, is involved in the defense against oxidative DNA damage. *J. Cell Biol.* 177:969–979. https://doi.org/10.1083/jcb.200701042

Tarín, J.J. 1996. Potential effects of age-associated oxidative stress on mammalian oocytes/embryos. *Mol. Hum. Reprod.* 2:717–724. https://doi.org/10.1093/molehr/2.10.717

Titus, S., F. Li, R. Stobezki, K. Akula, E. Unsal, K. Jeong, M. Dickler, M. Robson, F. Moy, S. Goswami, and K. Oktay. 2013. Impairment of BRCA1-related DNA double-strand break repair leads to ovarian aging in mice and humans. *Sci. Transl. Med.* 5:172ra21. https://doi.org/10.1126/scitranslmed.3004925

Toyooka, Y., N. Tsunekawa, Y. Takahashi, Y. Matsui, M. Satoh, and T. Noce. 2000. Expression and intracellular localization of mouse Vasa-homologue protein during germ cell development. *Mech. Dev.* 93:139–149. https://doi.org/10.1016/S0925-4773(00)00283-5

Tuppi, M., S. Kehrloesser, D.W. Coutandin, V. Rossi, L.M. Luh, A. Strubel, K. Hötte, M. Hoffmeister, B. Schäfer, T. De Oliveira, et al. 2018. Oocyte DNA damage quality control requires consecutive interplay of CHK2 and CK1 to activate p63. *Nat. Struct. Mol. Biol.* 25:261–269. https://doi.org/10.1038/s41594-018-0035-7

Wei, Z., J. Greaney, C. Zhou, and H. A Homer. 2018. Cdk1 inactivation induces post-anaphase-onset spindle migration and membrane protrusion required for extreme asymmetry in mouse oocytes. *Nat. Commun.* 9:4029. https://doi.org/10.1038/s41467-018-06510-9

Wiebusch, L., and C. Hagemeier. 2010. p53- and p21-dependent premature APC/C-Cdh1 activation in G2 is part of the long-term response to genotoxic stress. *Oncogene.* 29:3477–3489. https://doi.org/10.1038/onc.2010.99

Winship, A.L., J.M. Stringer, S.H. Liew, and K.J. Hutt. 2018. The importance of DNA repair for maintaining oocyte quality in response to anti-cancer treatments, environmental toxins and maternal ageing. *Hum. Reprod. Update.* 24:119–134. https://doi.org/10.1093/humupd/dmy002

Woods, L.M., C.A. Hodges, E. Baart, S.M. Baker, M. Liskay, and P.A. Hunt. 1999. Chromosomal influence on meiotic spindle assembly: abnormal meiosis I in female Mlh1 mutant mice. *J. Cell Biol.* 145:1395–1406. https://doi.org/10.1083/jcb.145.7.1395
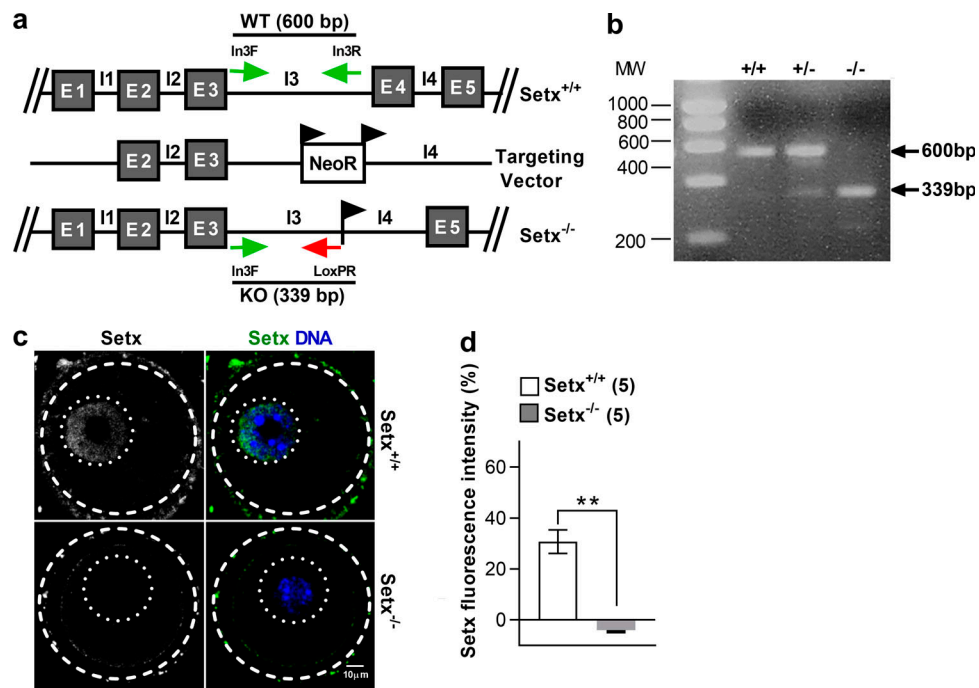
Supplemental material

Figure S1. **Targeted deletion of *SETX* gene and oocyte Setx expression. (a)** Schematic representation of the wild-type *SETX* allele, the targeting vector with the neomycin resistance (NeoR) cassette, and the Setx knockout (Setx$^{-/-}$) allele. The primers (ln3F, ln3R, and LoxPR) used and the sizes of the predicted PCR products obtained for wild type (WT; 600 bp) and knockout (KO; 339 bp) alleles are shown. E, exon; I, intron. Triangles denote the LoxP sites. **(b)** Products produced by undertaking PCR using primers in panel a on whole genomic DNA obtained from tail-tips of Setx$^{+/+}$, Setx$^{+/-}$, and Setx$^{-/-}$ animals. **(c)** Representative images of Setx$^{+/+}$ and Setx$^{-/-}$ oocytes immunostained for Setx and DNA. Outer dashed circle outlines the oocyte; inner dotted circle outlines the GV. Scale bar, 10 μm. **(d)** Quantification of Setx fluorescence intensity within the GV. Oocyte numbers are shown in parentheses. Error bars depict mean ± SEM. Two-tailed Student's *t* test used for statistical analysis. **, P < 0.01.
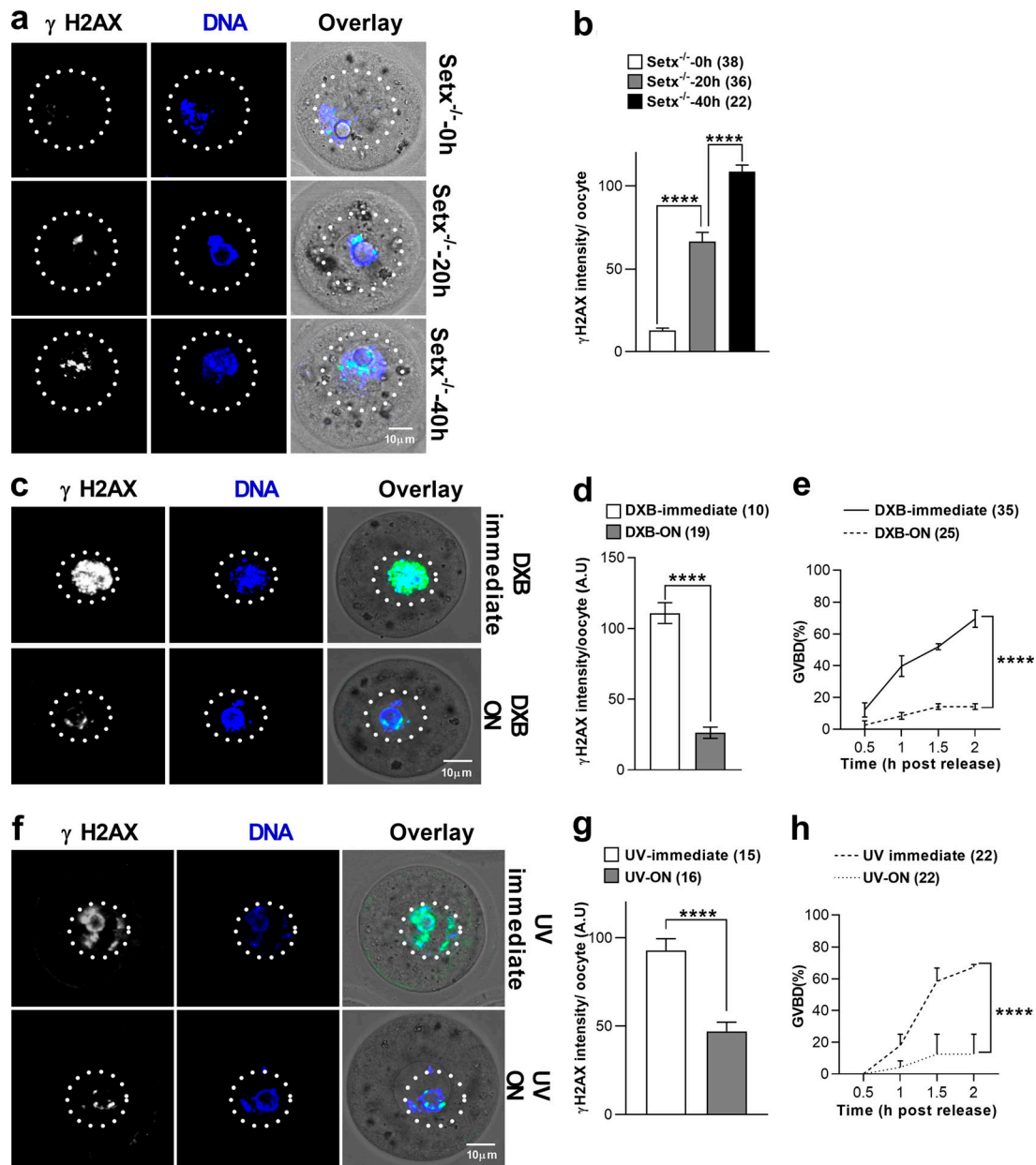
Figure S2. **DNA damage in Setx$^{-/-}$ oocytes during in vitro culture and response to treatment with either DXB or UV-B irradiation. (a and b)** Representative images of γH2AX and DNA labeling (a) and quantification of γH2AX intensity (b) in Setx$^{-/-}$ oocytes immediately after harvesting (0 h) and after 20 and 40 h in vitro culture. **(c and d)** Representative images of γH2AX and DNA labeling (c) and quantification of γH2AX intensity (d) in DXB-immediate and DXB-ON oocytes. **(e)** GVBD rates for DXB-immediate and DXB-ON oocytes. **(f and g)** Representative images of γH2AX and DNA labeling (f) and quantification of γH2AX intensity (g) in UV-immediate, and UV-ON oocytes. **(h)** GVBD rates for UV-immediate and UV-ON oocytes. Oocyte numbers are shown in parentheses. Error bars are mean ± SEM. Two-tailed Student's t test (b, d, and g) or two-way ANOVA (e and h) was used for statistical analysis. ***, P < 0.001; ****, P < 0.0001.
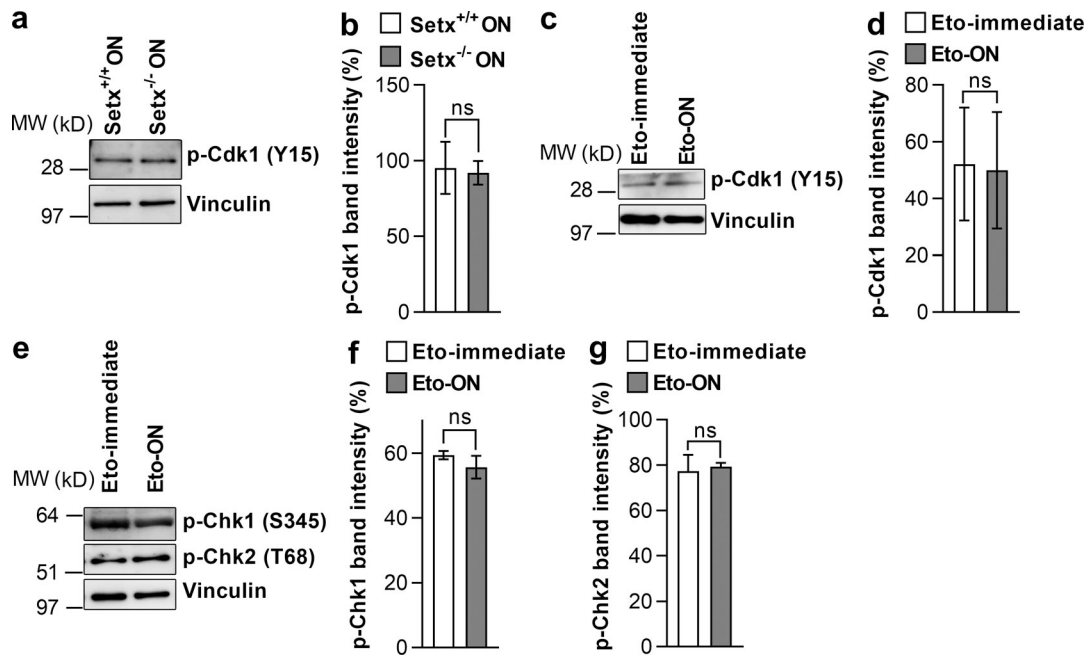
Figure S3. **G2 arrest was not due to the canonical phosphorylation pathway. (a–d)** Representative immunoblots (a and c) and quantification of p-Cdk1(Y15) (b and d) band intensities in Setx^{+/+}-ON and Setx^{−/−}-ON oocytes and Eto-immediate and Eto-ON oocytes (65 oocytes/group). **(e–g)** Representative immunoblots (e) and quantification of p-Chk1(S345) (f) and p-Chk2(T68) (g) band intensities in Eto-immediate and Eto-ON oocytes (60 oocytes/group). Data are from a minimum of three independent experiments. Error bars are mean ± SEM. Two-tailed Student's t test was used for statistical analysis. ns, P > 0.05.
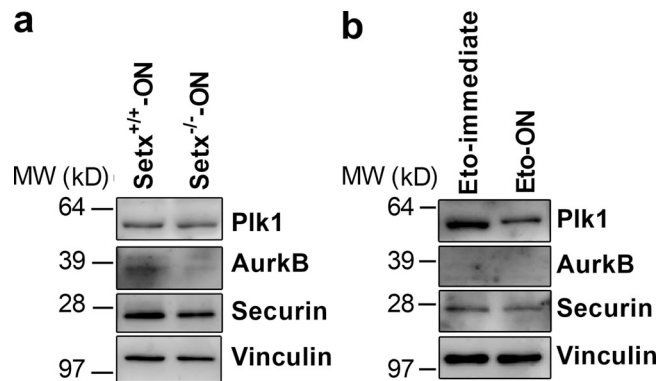

Figure S4. **Reduced levels of APC-Cdh1 substrates in Setx^{−/−}-ON and Eto-ON oocytes. (a and b)** Representative immunoblots of Plk1, Aurora kinase B (AurkB), and securin in Setx^{+/+}-ON and Setx^{−/−}-ON oocytes (a) as well as Eto-immediate and Eto-ON oocytes (b). Vinculin in blots served as a loading control.
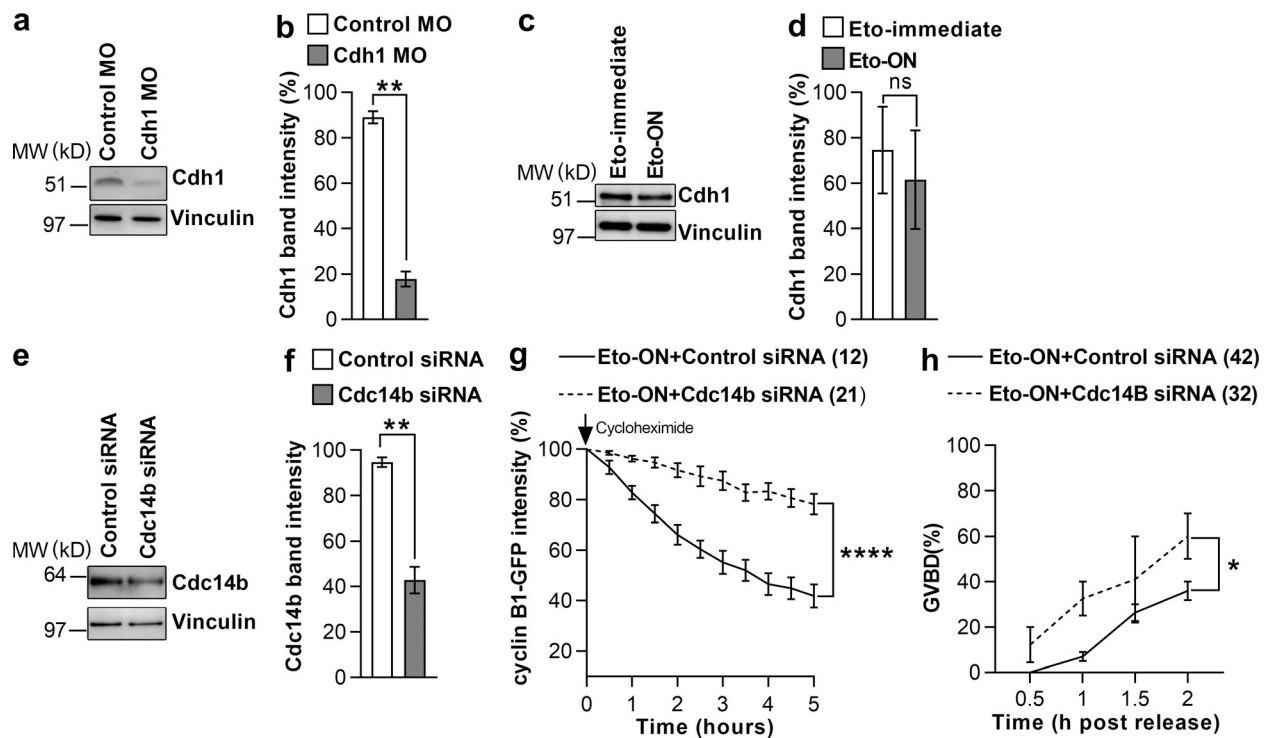
Figure S5. **Morpholino-induced depletion of Cdh1, Eto treatment does not affect Cdh1 levels, and Cdc14B activity increases following DNA damage and inhibits M-phase entry. (a and b)** Representative immunoblot (a) and quantification of Cdh1 band intensities (b) in oocytes injected with either a control morpholino (Control MO) or a *CDH1*-targeting morpholino (Cdh1 MO; 30 oocytes/group). **(c and d)** Representative immunoblot (c) and quantification of Cdh1 band intensities (d) in Eto-immediate and Eto-delay GV-stage oocytes (30 oocytes/group). **(e–g)** Representative immunoblot (e) and quantification of Cdc14B band intensities (f) in GV-stage oocytes microinjected with either control or *CDC14B*-targeting siRNAs (30 oocytes/group). Quantification of cyclin B1-GFP fluorescence (g) in Eto-ON oocytes microinjected with either control or *CDC14B*-targeting siRNAs. **(h)** GVDB rates for Eto-ON oocytes injected with either control or *CDC14B*-targeting siRNAs. Vinculin in blots served as a loading control. Oocyte number are shown in parentheses from a minimum of three independent experiments. Error bars are mean ± SEM. Two-tailed Student's *t* test (b, d, and f) or two-way ANOVA (g and h) was used for statistical analysis. ns, $P > 0.05$; *, $P < 0.05$; **, $P < 0.01$; ****, $P < 0.0001$.

Subramanian et al.
Oocytes possess a G2/M DNA damage checkpoint

Journal of Cell Biology   S4
https://doi.org/10.1083/jcb.201907213